Monthly Notices
of the
ROYAL ASTRONOMICAL SOCIETY

MNRAS **485,** 5294–5318 (2019)
Advance Access publication 2019 February 25

doi:10.1093/mnras/stz530

A multiwavelength analysis of a collection of short-duration GRBs observed between 2012 and 2015

S. B. Pandey,[1]★ Y. Hu,[2] Ao . J. Castro-Tirado,[2,3] A. S. Pozanenko,[12,13,36] R. Sánchez-Ramírez,[2,38] J. Gorosabel,[2,4,5] S. Guziy,[2,6,7] M. Jelinek,[2,9] J. C. Tello,[2] S. Jeong,[2,8] S. R. Oates,[2,41] B.-B. Zhang,[2,39,40]★ E. D. Mazaeva,[12] A. A. Volnova,[12] P. Yu. Minaev,[12] H. J. van Eerten,[42] M. D. Caballero-García,[9,2] D. Pérez-Ramírez,[10] M. Bremer,[11] J.-M. Winters,[11] I. H. Park,[8] A. Nicuesa Guelbenzu,[14] S. Klose,[14] A. Moskvitin,[15] V. V. Sokolov,[15] E. Sonbas,[16] A. Ayala,[2] J. Cepa,[17] N. Butler,[18] E. Troja,[19] A. M. Chernenko,[12] S. V. Molkov,[12] A. E. Volvach,[20] R. Ya. Inasaridze,[21,43] Sh. A. Egamberdiyev,[22] O. Burkhonov,[22] I. V. Reva,[23] K. A. Polyakov,[24] A. A. Matkin,[25] A. L. Ivanov,[26] I. Molotov,[37] T. Guver,[27] A. M. Watson,[44] A. Kutyrev,[19] W. H. Lee,[44] O. Fox,[30] O. Littlejohns,[18] A. Cucchiara,[19] J. Gonzalez,[44] M. G. Richer,[28] C. G. Román-Zúñiga,[28] N. R. Tanvir,[29] J. S. Bloom,[30] J. X. Prochaska,[31] N. Gehrels,[19] H. Moseley,[19] J. A. de Diego,[44] E. Ramírez-Ruiz,[31] E. V. Klunko,[32] Y. Fan,[33] X. Zhao,[33] J. Bai,[33] Ch. Wang,[33] Y. Xin,[33] Ch. Cui,[34] N. Tungalag,[35] Z.-K. Peng,[40] Amit Kumar,[1] Rahul Gupta,[1] Amar Aryan,[1] Brajesh Kumar,[1] L. N. Volvach,[20] G. P. Lamb[29] and A. F. Valeev[15]

Affiliations are listed at the end of the paper

Accepted 2019 February 19. Received 2019 February 19; in original form 2018 August 30

ABSTRACT

We investigate the prompt emission and the afterglow properties of short-duration gamma-ray burst (sGRB) 130603B and another eight sGRB events during 2012–2015, observed by several multiwavelength facilities including the Gran Canarias Telescope 10.4 m telescope. Prompt emission high energy data of the events were obtained by *INTEGRAL*-SPI-ACS, *Swift*-BAT, and *Fermi*-GBM satellites. The prompt emission data by *INTEGRAL* in the energy range of 0.1–10 MeV for sGRB 130603B, sGRB 140606A, sGRB 140930B, sGRB 141212A, and sGRB 151228A do not show any signature of the extended emission or precursor activity and their spectral and temporal properties are similar to those seen in case of other short bursts. For sGRB 130603B, our new afterglow photometric data constrain the pre-jet-break temporal decay due to denser temporal coverage. For sGRB 130603B, the afterglow light curve, containing both our new and previously published photometric data is broadly consistent with the ISM afterglow model. Modeling of the host galaxies of sGRB 130603B and sGRB 141212A using the LePHARE software supports a scenario in which the environment of the burst is undergoing moderate star formation activity. From the inclusion of our late-time data for eight other sGRBs we are able to: place tight constraints on the non-detection of the afterglow, host galaxy, or any underlying 'kilonova' emission. Our late-time afterglow observations of the sGRB 170817A/GW170817 are also discussed and compared with the sub-set of sGRBs.

Key words: gamma-rays: general – X-ray: bursts – techniques: photometric – radiation mechanims : non-thermalonova.

★ E-mail: shashi@aries.res.in (SBP); bbzhang@nju.edu.cn (BBZ)

1 INTRODUCTION

Short-duration gamma-ray bursts (sGRBs) were originally classified using the *Konus* catalogue (Mazets et al. 1981) that preceded the wider realization that sGRBs likely are binary compact mergers (Narayan, Paczynski & Piran 1992; Nakar 2007) based on various observed properties like duration, fluence etc. as described in Kouveliotou et al. (1993) and Bromberg et al. (2013). During the era of the Neil Gehrels *Swift* observatory, arcsec X-ray Telescope (XRT) localizations enabled the discovery of the first afterglow of sGRB 050509B (Castro-Tirado et al. 2005; Gehrels et al. 2005) and subsequently other observed features like extended emission (EE) at *Swift* Burst Alert Telescope (BAT) energies, temporally extended variable X-ray emission suggesting late time central engine activity due to either merger of two neutron stars (NS–NS) or a neutron star and a stellar mass black hole (NS–BH) as possible progenitors (Eichler et al. 1989; Narayan, Paczynski & Piran 1992; Usov 1992; Zhang & Meszaros 2001; Troja et al. 2007; Rowlinson, et al. 2013; D'Avanzo et al. 2014; Gibson et al. 2017; Desai, Metzger & Foucart 2018). The physical nature of the EE, observed in some of the sGRBs, is not yet resolved. It could be connected with the beginning of the afterglow phase (Minaev, Pozanenko & Loznikov 2010), the activity of a magnetar, formed during merger process (Metzger, Piro & Quataert 2008) or viewing angle effects (Barkov & Pozanenko 2011). The prompt emission properties of sGRBs, such as relatively harder spectra (higher $E_{\rm peak}$) and nearly zero spectral lag (Gehrels et al. 2006; Zhang et al. 2009), discriminate sGRBs from long GRBs (lGRBs). sGRBs have also been speculated as a potential key to understand gravitational wave (GW) sources and the nucleosynthesis of elements over the history of the Universe (Berger 2014; Kumar & Zhang 2015; Abbott et al. 2017a,b).

More than 90 afterglows of sGRBs have been detected at various wavelengths[1] exhibiting diverse properties (Lee & Ramirez-Ruiz 2007; Gehrels, Ramirez-Ruiz & Fox 2009; Berger 2014). Afterglows of sGRBs are in general less luminous and less energetic and favour typically lower circumburst densities than those seen in the case of lGRBs (Kann, Klose & Zhang 2011; Nicuesa et al. 2012; Berger 2014). Despite intensive efforts, this leads to a lower detection rate for sGRBs: ∼75 per cent in X-rays, ∼33 per cent in optica-NIR, and only a handful in the radio (Berger 2014). In comparison to long ones, sGRBs are observed to occur at over a lower and narrower redshift range ($z \sim 0.1$–1.5) and both early and late-type galaxies have been identified as hosts (Fong et al. 2013). Afterglow observations of sGRBs also indicate that these bursts have a range of jet-opening angles (Burrows et al. 2006; Kann et al. 2011; Nicuesa Guelbenzu et al. 2012; Fong et al. 2013; Zhang et al. 2015; Troja et al. 2016; Lamb & Kobayashi 2018; Margutti et al. 2018) and have systematically larger radial offsets from the host galaxies (Fong et al. 2013; Tunnicliffe et al. 2014) in turn supporting compact binary merger as possible progenitors (Bloom, Kulkarni & Djorgovski 2002; Zhang, Liang & Zhang 2007; Troja et al. 2008; Zhang et al. 2009; Salvaterra et al. 2010). Optical afterglows of sGRBs are generally fainter in comparison to those observed in the case of lGRBs, implying the need for fast and deep afterglow observations using moderate- to large-size telescopes.

Study of sGRBs now extends beyond understanding just about their explosion mechanisms, progenitors and environments. These explosions are now key to improve our understanding about multi-messenger astronomy and to search for new compact binary mergers as GW sources. It has been proposed that during the compact binary merger process, radioactive decay of heavy elements could give rise to a supernova-like feature, termed 'macronovae' or 'kilonovae' (Li & Paczynski 1998; Kulkarni 2005; Hotokezaka et al. 2013; Kasen, Fernandez & Metzger 2015) having a component of thermal emission caused by radioactive decay of elements through r-process nucleosynthesis. So far, tentative 'kilonova' like signatures have been identified in only a few cases including sGRB 050709 (Zhi-Ping et al. 2016), sGRB 060614 (Yang et al. 2015), sGRB 080503A (Perley et al. 2009), sGRB 130603B (Hotokezaka et al. 2013; Tanvir et al. 2013), sGRB 150101B (Fong et al. 2016; Troja et al. 2018), sGRB 160821B (Kasliwal et al. 2017), and recently sGRB 170817A/GW170817/AT 2017gfo (Abbott et al. 2017a,b). Discovery of the ground-breaking event called sGRB 170817A/GW170817/AT 2017gfo has opened new windows in the understanding of GWs: their electromagnetic counterparts (Abbott et al. 2017a; Albert et al. 2017), and their likely contribution to heavy element nucleosynthesis in the nearby Universe (Lattimer & Schramm 1974; Piran, Nakar & Rosswog 2013; Pian et al. 2017).

Multiwavelength observations of a larger sample of nearby sGRBs and 'kilonovae' features like GW170817/sGRB 170817A/AT 2017gfo are crucial to establish whether compact binary mergers are the progenitors (Kasen et al. 2015) for all such events (Abbott et al. 2017a,b) and to put a constraint on the electromagnetic counterparts and number density of GW sources in near future (Li & Paczynski 1998; Shibata & Taniguchi 2011; Loeb 2016).

In this paper, we present results based on prompt emission data from *INTEGRAL*, *Swift*, *Fermi*, and multiwavelength follow-up afterglow observations of nine sGRBs. The data sets were mostly not published yet and were observed by various different-size optical and NIR ground-based telescopes including the 10.4 m Gran Canarias Telescope (GTC). Observations of these nine bursts including sGRB 170817A were collected during 2012–2018 as a part of a large multiwavelength collaboration. Our analysis of new data for the subset of sGRBs mainly focused towards constraining prompt emission, afterglow, and host galaxy properties and adding value towards known physics behind these cosmic explosions. We also attempt to compare the observed properties of the subset of sGRBs with a new class of less-studied but associated events called 'Kilonovae'. The paper is organized as follows: in Sections 2 and 3 we present our own temporal and spectral analysis of the afterglow and host galaxy data of GRB 130603B alongside the published ones; in Section 4 and in Appendix 'A' we discuss the results of prompt emission and multiband afterglow observations of the other eight sGRBs, and in Section 5 we present late-time GTC observations of sGRB 170817A/GW170817/AT 2017gfo and compare the observed properties with the subset of the bursts presently discussed. Finally, in Section 6 we summarize the conclusions drawn from the analysis of all the sGRBs. In this paper, the notation $F_\nu(t) \propto t^{-\alpha}\nu^{-\beta}$ is used, where α is the flux temporal decay index and β is the spectral index. Throughout the paper, we use the standard cosmological parameters, $H_0 = 71\,{\rm km\,s^{-1}Mpc^{-1}}$, $\Omega_M = 0.27$, $\Omega_\Lambda = 0.73$.

2 SGRB 130603B, MULTIWAVELENGTH OBSERVATIONS

sGRB 130603B was discovered on 2013 June 3 at 15:49:14 UT by *Swift*-BAT (Barthelmy et al. 2013; Melandri et al. 2013), and by *Konus* − *Wind* (Golenetskii et al. 2013). The γ-ray light curve of GRB 130603B consists of a single group of pulses with a duration of $T_{90} = 0.18 \pm 0.02$ s (15–350 keV; Barthelmy et al. 2013). The

[1] http://www.astro.caltech.edu/grbox/grbox.php

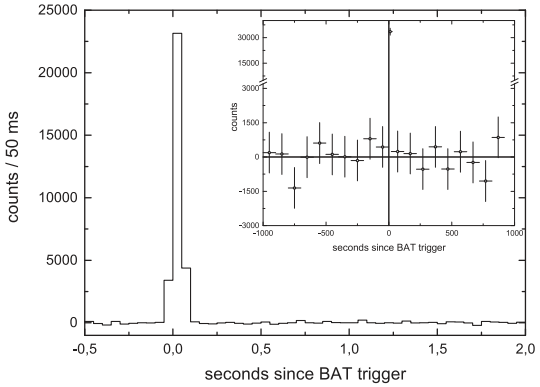

Figure 1. Background subtracted light curve of sGRB 130603B of *INTEGRAL* SPI-ACS in the energy range 0.1–10 MeV with 50 ms time resolution. The *x*-axis shows time since BAT trigger. Inset: light curve with time resolution of 100 s.

Konus − *Wind* fluence of the burst is $(6.6\pm0.7) \times 10^{-6}$ erg cm^{-2} (20–10^4 keV), with a peak energy of 660 ± 100 keV (Golenetskii et al. 2013). The reported measured value of $E_{\rm iso,\,\gamma} \sim 2.1 \times 10^{51}$ erg, places the burst well above the $E_{\rm peak}$-$E_{\rm iso}$ locus for long GRBs in the Amati diagram (Amati et al. 2008, also fig. 6). Such behaviour is often observed for short bursts (Minaev & Pozanenko 2019).

sGRB 130603B shows negligible spectral lag (Norris et al. 2013), typical for short bursts. Many authors (e.g. Hakkila & Preece, 2014; Minaev et al. 2014) have found a strong correlation between pulse duration and spectral lag: longer pulses have larger lags. The correlation is similar for both sGRBs and lGRBs. As sGRBs typically consist of shorter pulses than long ones, they have less significant spectral lags in general. GRB light curves often consist of several pulses including highly overlapping ones: spectral and temporal properties of individual pulses may be not adequately resolved (Chernenko 2011). By performing spectral lag analysis via the superposition of several overlapping pulses, one can obtain an unpredictable result because each pulse has unique spectral and temporal properties (Minaev et al. 2014). As a result, one can find negligible or negative lag under certain conditions even if each pulse has a positive (but unique) lag (for details, see Minaev et al. 2014). sGRB 130603B consists of several very short and overlapped pulses, so its negligible spectral lag may be connected with short duration of pulses while performing spectral lag analysis for superposition of several pulses.

2.1 SPI-ACS *INTEGRAL* observations

sGRB 130603B was also triggered by the INTEGRAL Burst Alert System (IBAS) system operating with spectrometer for *INTEGRAL*-anticoincidence system (SPI-ACS) (Fig. 1). SPI-ACS *INTEGRAL* has very high effective area (up to 0.3 m^2) in energy range > 100 keV and stable background at time-scales of hundreds of seconds (Minaev et al. 2010), which makes SPI-ACS a suitable instrument to study light curves of short-hard GRBs and especially to search for weak signals from their precursors and EE components. The off-axis angle of sGRB 130603B to the SPI-ACS axis is 103 deg, which is almost optimal for detection, making sGRB 130603B one of the brightest short bursts ever registered by SPI-ACS. Nevertheless, we do not find statistically significant EE in the SPI-ACS data (Inset in Fig. 1, in terms of peak flux at 50 ms time scale), which is in agreement with results obtained from *Swift*-BAT in the softer energy range of 15–150 keV (Norris et al. 2013). There is also no evidence for a precursor in SPI-ACS data during time-scales from 0.01s up to 5s, in agreement with the previous results (Troja, Rosswog & Gehrels 2010; Minaev & Pozanenko 2017; Minaev, Pozanenko & Molkov 2018).

In Vigano & Mereghetti (2009), it was shown that one SPI-ACS count corresponds on average to $\sim10^{-10}$ erg cm^{-2} in the (75, 1000) keV range, for directions orthogonal to the satellite pointing axis. Using the conversion factor, we can roughly estimate the flux values in the (75, 1000) keV range for GRBs observed by SPI-ACS. The fluence estimation of sGRB 130603B in SPI-ACS is ∼31 000 counts or $S_{\rm EE} \sim 3.1 \times 10^{-6}$ erg cm^{-2} in the (75, 1000) keV range, which is in agreement with Konus–Wind observations (Golenetskii et al. 2013). At a time-scale of 50s, the upper limit on EE activity for sGRB 130603B is ∼7100 counts ($S_{\rm EE} \sim 7 \times 10^{-7}$ erg cm^{-2}) at the 3σ significance level, the corresponding upper limit on precursor activity at a time-scale of 1s, is ∼1000 counts ($S_{\rm EE} \sim 10^{-7}$ erg cm^{-2}), both are in the (75, 1000) keV range.

2.2 Optical-IR photometric observations

As a part of this collaboration, photometric observations of the optical-IR afterglow and the host galaxy were performed using several facilities worldwide, including 1.0 m telescope at the Tubitak National Observatory (Antalya, Turkey); the 1.5 m telescope at Observatorio de Sierra Nevada (Granada, Spain); the AS-32 0.7 m telescope at Abastumani Astrophysical Observatory Georgia; the Reionization And Transients Infra-Red RATIR camera at the 1.5 m telescope of the San Pedro Martir observatory; the 2.0 m Liverpool telescope at La Palma; AZT-22 1.5 m at the Maidanak observatory Uzbekistan; the Centro Astronómico Hispano-Alemán (CAHA) 3.5 m located in Almeria (Spain); the newly commissioned 3.6 m Devasthal Optical Telescope (DOT) at Aryabhatta Research Institute of Observational Sciences (ARIES) Nainital, India, and with the 10.4 m Gran Telescopio Canarias (GTC), located at the observatory of Roque de los Muchachos in La Palma (Canary Islands, Spain), equipped with the Optical System for Imaging and low-Intermediate-Resolution Integrated Spectroscopy (OSIRIS) instrument. Our observations by the 1.0 m telescope at the Tubitak, starting ∼0.122d after the burst are the earliest reported ground-based observations so far for sGRB 130603B. All optical-NIR data were processed using DAOPHOT software of NOAO's IRAF package,[2] a general purpose software system for the reduction and analysis of astronomical data. The photometry was performed in comparison to nearby standard stars and image subtraction was applied whenever it was required to subtract the host galaxy contribution as exaplained in Alard & Lupton (1998). The unfiltered observations made with the AbAO AS-32 telescope have been considered equivalent to *r*-band as the quantum efficiency of the detector is at a maximum around *r*-band frequencies. The final AB magnitudes of the afterglow and the host galaxy in different pass-bands as a part of the present analysis are listed in Table 1.

2.3 Spectroscopic observations

A spectroscopic redshift at the location of the afterglow was obtained by several groups, including Xu et al. (2013), Foley et al. (2013), de Ugarte Postigo et al. (2013), and Cucchiara, Perley & Cenko (2013). As a part of the present study, spectroscopic

[2] http://iraf.noao.edu/

Table 1. Broad-band optical-IR photometric observations of the GRB 130603B afterglow and its host galaxy (h) presented in the AB-magnitude system. The values are not corrected for extinction and are tabulated in order of time in days (d) since the burst. The quoted values of limiting magnitude are 3σ.

t-t0, mid(d)	exp(s)	Afterglow/ Host magnitudes	Pass-band	Telescopes
0.1222	150 × 10	20.15 ± 0.17	R_c	Tubitak 1.0 m
0.1959	300 × 10	21.37 ± 0.25	*Clear*	AS-32 0.7 m
0.2024	300 × 4	21.10 ± 0.27	I_c	OSN 1.5 m
0.3360	50	21.29 ± 0.02	*i*	GTC 10.4 m
0.5196	3020.0	22.12 ± 0.81	Y	RATIR 1.5 m
0.5196	3020.0	20.37 ± 0.28	H	RATIR 1.5 m
0.5347	2818.0	21.64 ± 0.34	Z	RATIR 1.5 m
0.5347	2818.0	20.94 ± 0.38	J	RATIR 1.5 m
0.5405	6960.0	22.30 ± 0.20	*r*	RATIR 1.5 m
0.5405	6960.0	21.98 ± 0.20	*i*	RATIR 1.5 m
1.1141	150 × 2 + 200 × 8	21.34 ± 0.50	R_c	Tubitak 1.0 m
1.1160	180 × 14	> 22.64	*clear*	AS-32 0.7 m
2.0937	180 × 10	>22.92	R_c	Maidanak 1.5 m
2.1489	200 × 5	>21.14	R_c	Tubitak 1.0 m
2.2803	300 × 5	20.69 ± 0.15 (h)	I_c	OSN 1.5 m
5.1143	180 × 23	>22.56	*clear*	AS-32 0.7 m
16.2691	300 × 10	20.69 ± 0.06 (h)	*i*	LT 2.0 m
19.2650	60 × 15	19.69 ± 0.13 (h)	K_s	CAHA 3.5 m
19.2323	60 × 15	20.06 ± 0.09 (h)	J	CAHA 3.5 m
19.2481	60 × 15	19.68 ± 0.13 (h)	H	CAHA 3.5 m
19.2155	60 × 15	20.11 ± 0.07 (h)	Z	CAHA 3.5 m
32.2411	50 × 4	22.01 ± 0.03 (h)	*g*	GTC 10.4 m
32.2471	50 × 4	20.97 ± 0.01 (h)	*r*	GTC 10.4 m
32.2511	50 × 4	20.65 ± 0.02 (h)	*i*	GTC 10.4 m
35.5168	469.8	20.88 ± 0.41 (h)	Y	RATIR 1.5 m
35.5168	469.8	20.84 ± 0.30 (h)	H	RATIR 1.5 m
35.5168	335.6	20.39 ± 0.19 (h)	Z	RATIR 1.5 m
35.5168	335.6	20.49 ± 0.43 (h)	J	RATIR 1.5 m
35.5162	960.0	21.26 ± 0.12 (h)	*r*	RATIR 1.5 m
35.5162	960.0	20.79 ± 0.09 (h)	*i*	RATIR 1.5 m
1387.84	300.0 × 2	22.13 ± 0.05 (h)	*B*	3.6 m DOT
1387.86	300.0 × 2	20.72 ± 0.02 (h)	R_c	3.6 m DOT

observations were performed to measure the redshift of sGRB 130603B independently and are reported in Sánchez-Ramírez et al. (2013).

We obtained optical spectra with the GTC(+ OSIRIS) starting at 23:58 h. Observations consisted of two 450 s exposures, one with each of the R1000B and R500R grisms, using a slit of width 1.2 arcsec. Data reduction was performed using standard routines from the Image Reduction and Analysis Facility (IRAF). The afterglow spectrum shows Ca II in absorption, and we detect a significant contribution from the underlying host galaxy (e.g. [O II], [O III], Hβ and Hα emission lines about 1' offset), together implying a redshift of $z = 0.356 \pm 0.002$, consistent with the values provided by de Ugarte Postigo et al. (2013) and Foley et al. (2013). The reduced spectrum obtained at the location of the afterglow along with the lines identified are shown in Fig. 2. Using our redshift value and the fluence published by Golenetskii et al. (2013), the isotropic-equivalent gamma-ray energy is $E_{\mathrm{iso},\gamma} \sim 2.1 \times 10^{51}$ erg (20– 10^4 keV, rest-frame).

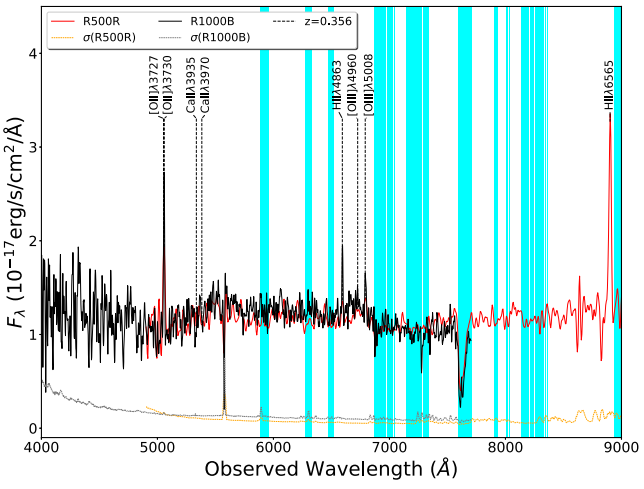

Figure 2. Spectroscopic observations of the sGRB 130603B at the location of the afterglow taken by the 10.4 m GTC (+ OSIRIS) using grisms R1000B and R500R starting ∼8 h after the burst (Sánchez-Ramírez et al. 2013). Telluric absorption bands are marked as cyan.

2.4 mm-wavelength observations

The afterglow of sGRB 130603B was observed with the Plateau de Bure Interferometer (Guilloteau et al. 1992), one of the largest observatories in the Northern Hemisphere operating at millimetre wavelengths (1, 2, and 3 mm). Observations were performed in

a four-antenna extended configuration for the first epoch whereas a five-antenna configuration on the consecutive dates as listed in Table 2. The data reduction was done with the standard CLIC and MAPPING software distributed by the Grenoble GILDAS group. Flux calibration includes a correction for atmospheric decorrelation that has been determined with a UV plane point source fit to the phase calibration quasar 1156 + 295. The carbon star MWC349 was used as the primary flux calibrator due to its well-known millimetre spectral properties (see e.g. Schwarz 1978). The burst location was also followed up using the RT-22 radio telescope of CrAO (Crimea) at 36 GHz and the data reduced using the standard software routines (Villata et al. 2006) and used modulated radiometers in combination with the registration regime 'ON–ON' for collecting data from the telescope (Nesterov, Volvach & Strepka 2000). The upper limits based on these observations are also given in Table 2. As a part of the present analysis, upper limits (1σ) based on IRAM Plateau de Bure Interferometer observations of sGRB 140606A, sGRB 140622A, and sGRB 140903A using the carbon star MWC349 as the primary flux calibrator are also tabulated in Table 2.

Observations at mm-wavelengths are very important as they suffer negligible absorption or interstellar scintillation effects, so sGRBs at high redshifts or highly extinguished bursts could be observed. It is expected that emission at mm-wavelengths is normally above the self-absorption frequency and lies around peak of the GRB synchrotron spectrum, allowing to probe for possible reverse shock emission at early epochs and to constrain afterglow models observed recently in case of many lGRBs (de Ugarte Postigo et al. 2012; Perley et al. 2014).

In Fig. 3, observed mm-wavelength upper limits of four sGRBs presented in Table 2 were plotted along with previous observations of another five sGRBs (namely sGRB 020531, sGRB 050509B, sGRB 051105A, sGRB 060801, and sGRB 080426, data taken from Castro-Tirado et al. 2019) and were compared with the afterglow light curve of a well-known nearby and bright lGRB 130427A observed at 3 mm (Perley et al. 2014). It is clear from Fig. 3 that using PdBI, we have been able to observe nine sGRBs so far but none was detected at mm-wavelengths in contrast with lGRBs that have been detected in many cases constraining various physical models (de Ugarte Postigo et al. 2012; Perley et al. 2014). Out of these nine sGRBs, only sGRB 130603B (Fong et al. 2014a) and sGRB 140903A (Troja et al. 2016) were detected at VLA radio frequencies so far. However, as discussed further in this work, the observed 3-mm PdBI 1σ upper limits for these two bursts are consistent with those predicted by the forward shock afterglow models. The gamma-ray fluence and observed X-ray flux values for these nine sGRBs are similar to those observed in case of other sGRBs. Non-detections of these nine sGRBs at 3 mm in the last decade using PdBI and other mm-wavelength facilities globally are helpful to constrain underlying physics behind these energetic sources and demand for more sensitive and deeper follow-up observations.

3 PROPERTIES OF SGRB 130603B

3.1 Afterglow light curves and comparison to models

Fig. 4 shows the r and i pass-band light curves of the sGRB 130603B afterglow including data from the present analysis and those published in the literature (Berger, Fong & Chornock 2013; Cucchiara et al. 2013a; Tanvir et al. 2013; de Ugarte Postigo, Thone & Rowlinson 2014). To plot the light curves along with those published in the literature, the data were scaled to respective AB magnitudes in SDSS r and i bands (see Fig. 4). The R_c band data taken at ∼0.122d comprise of the earliest reported ground-based detection and the remaining data fill the temporal gap in the light curve for this interesting short-duration burst. From the present analysis, the number of new data points in both r and i bands are four each spread up to ∼2.3d post-burst. Careful image-subtraction and calibration of the afterglow data < 0.23d post-burst indicates possible deviations from smooth power-law behaviour during the first few hours.

To determine the temporal flux decay slopes and the break time, we fitted an empirical function representing a broken power law, $F_\nu = A[(t/t_b)^{s\alpha_1} + (t/t_b)^{s\alpha_2}]^{-1/s}$ (Beuermann et al. 1999) to the r band combined light curve. The quantities α_1 and α_2 are asymptotic power-law flux decay slopes at early and late times with $\alpha_1 < \alpha_2$. The parameter $s > 0$ controls the sharpness of the break and t_b is the break time. The best fit of this broken power-law function to the r-band data including the very first data point taken at ∼0.122d gives $\alpha_1 = 0.81 \pm 0.14$; $\alpha_2 = 2.75 \pm 0.28$ and $t_b = 0.41 \pm 0.04$ with $\tilde{\chi}^2/dof = 2.22$ for a value of the smoothing parameter $s = 4$. The values of t_b and α_2 are similar to those derived by Fong et al. (2014a). Although the data from *Swift* XRT is consistent with a break occurring around 0.3 days, the later XMM-Newton observations suggest no turnover at X-ray frequencies and a continuing power law instead (this 'X-ray excess' is also discussed by Fong et al. (2014a)). The present analysis also helped to constrain the value of α_1 using a single-band light curve and found to be shallower in comparison to that derived by Fong et al. (2014a).

The present data set has also been used to constrain the spectral energy distribution (SED) of the afterglow. The RATIR data taken simultaneously at ∼0.52d post-burst (see Table 1) require an optical-NIR spectral index $\beta_{\rm opt} \sim 0.7$ once corrected for Galactic and considerable host extinction, similar to those measured by de Ugarte Postigo et al. (2014) at ∼0.35d and by Fong et al. (2014a) at ∼0.6d post-burst. The optical-NIR spectral index, together with the published value of the XRT spectral index $\beta_X = 1.2 \pm 0.1$, is consistent with $\Delta\beta = \beta_X - \beta_{\rm opt} = 0.5$, as expected in the case of a slow-cooling synchrotron spectrum (Sari, Piran & Narayan 1998) where the optical and XRT frequencies lie in two different spectral regimes.

Additionally, the derived values of the temporal slope α_1 and the spectral slope $\beta_{\rm opt}$ above are consistent with the closure relation $\beta = 3\alpha/2$ in the case of adiabatic deceleration in the interstellar medium *ISM* afterglow model for the spectral regime $\nu_{\rm m} < \nu < \nu_{\rm c}$, where $\nu_{\rm m}$ is the break frequency corresponding to the minimum electron energy and $\nu_{\rm c}$ is the cooling break frequency. The temporal flux decay index $\alpha_2 = 2.75 \pm 0.28$, the break-time $t_{\rm b} = 0.41 \pm 0.04$ and estimated slopes of the SEDs using the optical-NIR and XRT data are broadly consistent with the scenario described by Rhoads (1999) where the edge of the relativistic outflow causes a steepening (jet-break) in the observed light curve by t^{-p} (Sari, Piran & Halpern 1999), where p is the electron energy index. Also, for the observed XRT frequencies that lie above $\nu_{\rm c}$, the temporal and spectral indices are consistent with the predictions made by the *ISM* model in case of the adiabatic deceleration for the data up to 1 day post-burst (de Ugarte Postigo et al. 2014; Fong et al. 2014a).

Present afterglow data have made it possible to construct a single-band afterglow light curve and do the temporal fitting to derive parameters like temporal indices and jet-break time. The optical afterglow data in r and i bands from the present analysis have allowed us to construct a better-sampled light curve of the sGRB 130603B and to constrain the value of the pre-jet-break temporal decay index α_1 for the first time using data from a single band. This overall analysis supports the scenario that the observed steepening in the optical light curves is a jet-break as predicted theoretically

Table 2. Millimetre wave observations of the sGRB 130603B, sGRB 140606A, sGRB 140622A, and sGRB 140903A (1σ upper limits) afterglows as observed by Plateau de Bure Interferometer (PdBI) and centimetre wave observations using RT-22 in Crimea.

Start time	End time	Centre t-t0(d)	Frequency (GHz)	Flux centre (mJy)	Telescopes
		sGRB 130603B			
2013 June 03.844	03.926	03.901	86.743	+0.051 ± 0.120	PdBI
2013 June 04.826	03.908	04.867	86.743	−0.307 ± 0.095	PdBI
2013 June 12.721	12.828	12.775	86.743	−0.043 ± 0.073	PdBI
2013 June 04.730	04.801	04.765	36.0	1.6 ± 0.9	RT-22
2013 June 05.703	05.732	05.717	36.0	1.9 ± 1.2	RT-22
2013 June 05.710	05.785	05.747	36.0	2.6 ± 0.9	RT-22
		sGRB 140606A			
2014 June 14.039	14.099	14.069	86.743	0.331 ± 0.187	PdBI
2014 June 15.039	15.099	15.069	86.743	−0.592 ± 0.214	PdBI
		sGRB 140622A			
2014 June 26.050	26.108	0.079	86.243	−0.376 ± 0.123	PdBI
		sGRB 140903A			
2014 Sep 05.617	05.705	02.661	86.743	0.120 ± 0.130	PdBI

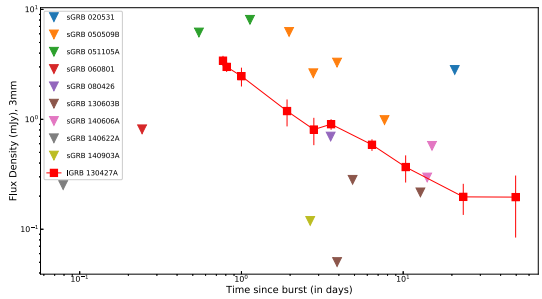

Figure 3. Comparison of the 3-mm afterglow light curve of nearby lGRB 130427A (Perley et al. 2014) to the present set of mm-wavelength upper limits (1σ) of four sGRBs (from Table 2) along with another set of upper limits of 5 sGRBs as discussed in Castro-Tirado et al. (2019) placed at a common redshift of $z = 0.34$.

by Sari et al. (1999) and Rhoads (1999). However, the observed X-ray excess emission (Fong et al. 2014a) for epochs $>$ 1d is not supported by the afterglow model.

3.2 Afterglow SED at the epoch of mm observations

Based on the present analysis and using the afterglow data in X-ray, *r*, *i* bands and the results published by de Ugarte Postigo et al. (2014) and Fong et al. (2014a), an afterglow SED was constructed for the epoch of our earliest millimeter observations i.e. 0.22d after the burst (see Fig. 5). We first built a time-sliced X-ray spectrum from the Leicester XRT webpages,[3] extracting data in the range 10ks–18ks after the trigger. This tool provides the appropriate spectral and response files that are compatible for use with the spectral fitting package XSPEC. The source spectral file was normalized so that it has the same count rate as a single epoch spectrum measured at 0.22d (see Schady et al. 2010 for details). For the optical data, we created appropriate spectral and response files for each filter. The flux values at 0.22d for each spectral file were determined from an extrapolation/interpolation the data between 10ks and 30ks by

[3]http://www.swift.ac.uk/xrt_spectra/

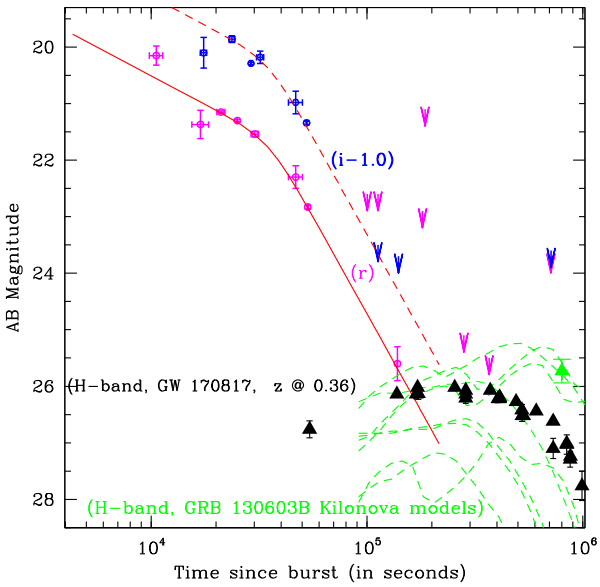

Figure 4. Afterglow optical *r* (pink) and *i* (blue) pass-band light curves of the sGRB 130603B. The solid red curves are the best-fit broken power-law model to the *r*-band light curves as described above. The red dashed line is the model over-plotted on the *i*-band light curve to guide eyes. The green triangle in the right bottom corner is the single point detection of the underlying 'kilonova' detection as described in Tanvir et al. (2013). The green dashed lines are the *H*-band 'kilonova' models at the redshift of ∼0.36 as taken from Tanaka et al. (2014). The black triangles are the *H*-band light curve (at redshift $z = 0.36$) of the electromagnetic counterpart of the recently discovered GW170817 (sGRB 170817A/AT 2017gfo) for comparisons as compiled in Villar et al. (2017a).

fitting a power law and fixing the slope as 0.81. This is the decay index found for the first segment of the broken power-law fit to the *r*-band data. The optical errors were estimated by taking the average error of the data between 10 and 30ks and adding a 5 per cent systematic error in quadrature.

The SEDs were fitted using XSPEC, following the procedure outlined in Schady et al. (2010, 2007). We fit two different models,

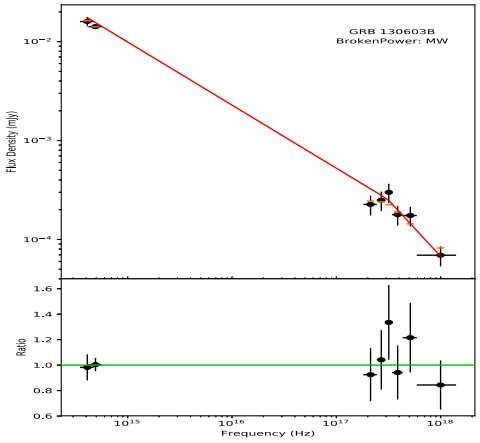

Figure 5. X-ray and optical SED of sGRB 130603B at the epoch of first millimetre observations i.e. 0.22d after the burst. We plot the best-fitting absorption and extinction corrected spectral model (solid red lines, broken power-law model), as well as the host galaxy absorbed and extinguished spectral model (orange dash lines) and the data (black circles) using the method described in Schady et al. (2010).

a power law and broken power law, which include Galactic and host galaxy absorption and extinction components (phabs, zphabs, and zdust). The best-fitting results obtained using the procedure mentioned above are plotted in Fig. 5, which supports broken power-law model for Milky Way (MW) type of host extinction. Values of the best-fitting borken power-law model and MW type of host extinction are consistent with those derived by de Ugarte Postigo et al. (2014). Assuming $\nu_{\rm m}$ around mm-wavelengths, 86.7 GHz upper limits of the sGRB 130603B at 0.22d post-burst (see Table 2) are also consistent with the extrapolated modeled flux values.

3.3 Broad-band modeling of sGRB 130603B afterglow

The multiband afterglow data of sGRB 130603B discussed above along with those published in Fong et al. (2014a) were used to fit numerical-simulation-based model to constrain physical parameters of the jetted emission as described in Zhang et al. (2015). The numerical modeling (Zhang et al. 2015) calculates the flux density at any frequency and observer time. The Monte Carlo method is used to determine the best parameter values (i.e. with the smallest χ^2 value) utilizing the MultiNest algorithm from Feroz, Hobson & Bridges (2009). The optical-NIR data were corrected for the Galactic and host extinction values as constrained in Fong et al. (2014a). The XRT data were also corrected for absorption effects. Based on the literature, it was decided to utilize the data 1000s after the burst for the modeling to avoid possible prompt emission effects at early epochs as described in Zhang et al. (2015).

Using the model and initial guess values, following set of parameter values were determined: the blast wave total energy $E_{\rm iso,\,53}$ (in the units of 10^{53} ergs), the ambient number density n, the electron energy density fraction $\epsilon_{\rm e}$, the magnetic field energy density fraction ϵ_B, the electron energy index p, and values of jet opening angle $\theta_{\rm jet}$ and the observed angle $\theta_{\rm obs}$. The best-fitting light curves obtained at different wavelengths are plotted in Fig. 6, the Monte Carlo parameter distributions are plotted in Fig. 7, and the resulting best-fit parameters and their uncertainties are listed in Table 3. A cross-check using an updated version of the SCALEFIT

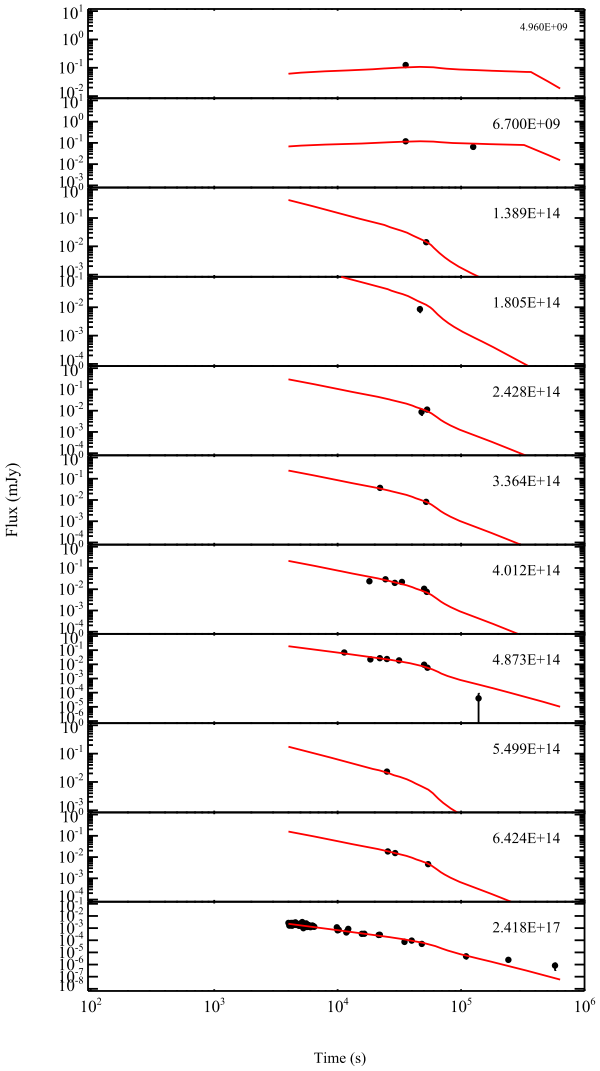

Figure 6. The best-fitting modeled multiband light curves determined from the numerical simulations as described above (Zhang et al. 2015). The corresponding frequency is marked on the right corner in each panel in the unit of Hz. The x-axis is the time since trigger in units of seconds. The observed flux density of each instrument is on the y-axis in units of mJy. All data were corrected for MW and host galaxy absorption and extinction effects before modeling. Red solid lines represent the modeled light curves.

package (van Eerten & MacFadyen 2012; Ryan et al. 2015) produces a similar jet opening angle and inferred energy.

Using the new data set discussed in this work, derived values of the physical parameters using present modeling method (Table 3) are constrained better than those reported by Fong et al. (2014a). The derived value of observed jet opening angle, $\theta_{\rm obs}$, is $\sim$3.2 deg. This value of $\theta_{\rm jet}$ gives rise to the beaming corrected $E_{\rm iso,\,53}$ is $\sim 1.4 \times 10^{49}$ erg. It is also clear from the present modeling that the best-fitting model was unable to reproduce the very late time X-ray emission observed in case of sGRB 130603B as noticed by using *Chandra* observations (Fong et al. 2014a). It is also noted that values of the isotropic-equivalent gamma-ray energy is $E_{\rm iso}$ and the blast wave energy $E_{{\rm iso},\,\gamma}$ are comparable, which in turn indicates the GRB radiative efficiency η_γ to be $\sim$23 per cent (with an uncertainty of $\sim$4 per cent), one of the highest among the known sample of sGRBs (Lloyd-Ronning & Zhang 2004; Wang et al. 2015).

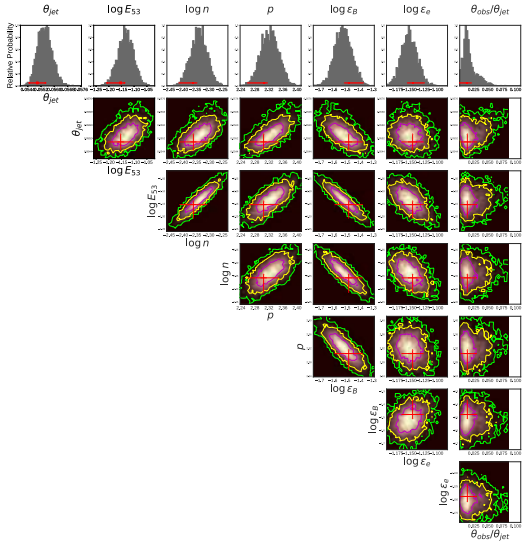

Figure 7. Triangle plot of the Monte Carlo fitting to our simulation-based model as described above (Zhang et al. 2015). It shows the posterior distribution and the correlation between the parameters.

Table 3. The best-fitting parameters of the numerical simulation (Zhang et al. 2015) to the multiwavelength afterglow data of sGRB 130603B.

Parameters	Value (−/+)
p	$2.31^{-0.01}_{+0.04}$
log$n$	$-2.36^{-0.01}_{+0.05}$
logϵ_e	$-1.14^{-0.02}_{+0.01}$
logϵ_B	$-1.47^{-0.11}_{+0.03}$
log$E_{\rm iso,\,53}$	$-1.15^{-0.01}_{+0.05}$
$\theta_{\rm jet}$	$0.055^{-0.001}_{+0.001}$
$\theta_{\rm obs}/\theta_{\rm jet}$	$0.014^{-0.06}_{+0.017}$

3.4 sGRB 130603B and 'kilonovae' connection

The 'kilonova' or 'macronova' events are electromagnetic transients powered by the radioactive decay of r-process elements synthesized in dynamical ejecta, and in the accretion disc winds during compact binary mergers where at least one component is a neutron star (Li & Paczynski 1998; Kulkarni 2005; Rosswog 2005). Compact binary mergers are also expected to be sources of GWs (Metgzer & Berger 2012; Nissanke, Mansi & Georgieva 2013; Tanaka & Hotokezaka 2013; Seigel & Ciolfi 2016a; Abbott et al. 2017a,b). For 'kilonovae', ejection of radioactive material during the merging process of the compact binaries could lead to an excess emission at optical-infrared or ultra-voilet frequencies. The brightness, duration, and spectrum of such emission is a function of the opacity, velocity, ejecta mass, and viewing angle (Metgzer et al. 2010; Bernes & Kasen 2013; Piran et al. 2013; Rosswog et al. 2014; Tanaka et al. 2014; Mooley et al. 2018; Radice et al. 2018). In turn, the opacity depends crucially on the neutron richness of the ejecta, which determines how far any r-process nucleosynthesis proceeds. The high-masst lanthanides, in particular, create heavy line-blanketing tha is expected to largely block out light in the optical bands. Recently, hydrodynamical modeling of such processes (Metzger & Fernandez 2014; Kasen et al. 2015) has predicted a brief early blue emission component produced in the outer lanthanide-free ejecta and a rather longer infrared transient produced in the inner lanthanide-blanketed regions at later epochs (Bulla et al. 2019). Using their disc-wind model for a case with a non-spinning black hole (Kasen et al. 2015), the optical bump observed in the case of sGRB 080503 (Perley et al. 2009) was interpreted in terms of an underlying 'kilonova' emission for an assumed redshift of $z = 0.25$. Their (Kasen et al. 2015) models were, however, unable to explain the observed infrared excess in sGRB 130603B, which required higher accretion disc mass and perhaps a rapidly spinning black hole (Fan, Yu & Xu 2013; Tanaka et al. 2014; Just et al. 2015). In this section, we attempt to place some constraints on the possible blue component of associated 'kilonova' based on the observed prompt emission and afterglow observations in bluer wavelengths for sGRB 130603B and their comparison with theoretical models.

It has been proposed by Barkov & Pozanenko (2011) that one should observe extended prompt emission in the case of sGRBs initiating Blandford–Znajek (BZ) jets (Blandford & Znajek 1977) due to large accretion disc mass and high accretion rate. However, in the case of sGRB 130603B EE was not detected (see Section 2 and Fig. 1). The absence of observable EE may indicate either that the observer is located off-axis with respect to the narrow BZ-jet, or that the accretion disc mass is small. In general, accretion disc mass should correlate with the ejected mass and the presence of EE could be an indicator of the emerging 'kilonovae' in sGRBs. Indeed, the plateau phase in X-ray emission observed in sGRB 130603B cannot be explained by a BZ-jet model (Kisaka & Ioka 2015) if we assume a small accretion disc mass. The absence of the EE and the presence of a plateau phase could be explained by a low accretion rate that has still initiated BZ jet but with moderate bulk relativistic gamma-factor. Alternatively, the magnetar model could explain the plateau phase of sGRB 130603B and 'kilonovae' features (Fan et al. 2013; Metzger & Piro 2014). Observing EE during the burst phase, along with the presence/absence of an early time X-ray plateau during afterglow phase for a larger sample of sGRBs, would allow discriminating among the possible progenitors as a subclass of compact-binary mergers producing magnetars (Zhang & Meszaros 2011; Rowlinson et al. 2013; Siegel & Ciolfi 2016a,b) but would also allow predicting some of them as potential candidates like GW170817.

In addition to the analysis described above, using published early-time afterglow data of sGRB 130603B in *Swift-UVOT u* and Gemini g' bands around ∼1.5d post-burst (de Ugarte Postigo et al. 2014), we attempt to constrain the possible early time blue emission contributing to the underlying 'kilonova'. The observed limiting magnitude in $u > 22.3$ mag and $g' > 25.7$ mag place limits on the corresponding luminosities of $L_u < 3.5 \times 10^{27}$ erg s^{-1} Hz^{-1} and $L_{g'} < 0.3 \times 10^{27}$ erg s^{-1} Hz^{-1}, respectively. Using the transformation equations (2) and (3) given in Tanaka (2016) (also see equations 7 and 8 in Fernandez & Metzger 2016), we tried to constrain the parameter called ejected mass $M_{\rm ej}$. However, these limiting values of luminosities in the two bands are not sufficiently deep to constrain values of the ejected mass meaningfully (>1.5 $M_\odot$) for the bluer component of 'kilonova' at the given epoch for the assumed values of the standard parameters. Considering the *WIND* models of 'kilonovae' with rather lower opacity and expansion velocities (Metzger & Fernandez 2014; Kasen et al. 2015; Tanaka 2016), constraints for the ejected mass $M_{\rm ej}$ are even weaker i.e. $M_{\rm ej} >$ a few $M_\odot$, which is unphysical. We caution that the placed limits on $M_{\rm ej}$ could be shallower if there were some contribution from the afterglow at the epoch of observations, which is certainly plausible. It is also worth mentioning that the some of parameters in the 'kilonovae'

models like the range spin of the neutron star, f-parameter, neutron richness have not been well-constrained so far (Metzger et al. 2010; Kasen et al. 2015), causing large uncertainty when predicting the possible emission at UV, optical, or IR frequencies. On the other hand, in case of recently observed underluminous and nearby event sGRB 170817A/GW170817, lanthanide-poor observed blue components were successfully modeled using a three-component 'kilonova' model (Villar et al. 2017a,b) with more realistic value of $M_{ej} \sim 0.016\ M_{\odot}$. So, present constraint on M_{ej} in case of sGRB 130603B indicates that either blue-component 'kilonova' emission was absent/weaker in comparison to the observed blue component in case of GW170817. These constraints further indicate that it could be possible to get a range of blue component of 'kilonovae' emission due to possible effects caused by a range of the dynamical ejecta, lifetime, and spin of the promptly formed magnetar/Black Hole, viewing angle effects etc. in case of some of the sGRBs. Early time deeper observations at bluer wavelengths for many such events at various distances are required to determine the range of properties like brightness, duration, and possible diversity among these events.

3.5 Host galaxy SED modeling of sGRB 130603B

Information about the host galaxy, such as the characteristic age of the dominant stellar population and the average internal extinction, was obtained by analyzing its broad-band SED (Table 4) using stellar population synthesis models. The host galaxy of GRB 130603B is a perturbed spiral galaxy as seen in high-resolution *HST* image (Tanvir et al. 2013) due to interaction with another galaxy. We combined our observational data in filters B, g, r, R_C, i, z, J, H, K_s obtained with GTC, CAHA, and DOT telescopes (see Table 1) and combined them with ultra-violet data in *uvw*2, *uvm*2, *uvw*1, *U* bands from de Ugarte Postigo et al. (2014) to construct the broad-band SED of the host galaxy. Taking into account a Galactic reddening along the line of sight of $E(B-V) = 0.02$ mag, and fixing the redshift of $z = 0.356$, we fitted the host SED using LEPHARE software package (Arnouts et al. 1999; Ilbert et al. 2006). We used the PEGASE2 population synthesis models library (Fioc & Rocca-Volmerange 1997) to obtain the best-fitted SED and the main physical parameters of the galaxy: type, age, mass, star-formation rate (SFR) etc. We tried different reddening laws: MW (Seaton 1979), LMC (Fitzpatrick 1986), SMC (Prévot et al. 1984), and the reddening law for starburst galaxies (Calzetti et al. 2000; Massarotti et al. 2001).

According to the best fit, the host is a type Sd galaxy with absolute magnitude in rest-frame $M_B = -20.9$, moderate bulk extinction of $E(B-V) = 0.2$, and MW dust extinction law. It is about 0.7 Gyr old, has a mass of $1.1 \times 10^{10}\ M_{\odot}$ and a low SFR of $\sim 6\ M_{\odot}\ yr^{-1}$. All the parameters are listed in Table 4. The reduced χ^2, galaxy morphological type, bulk extinction, absolute rest-frame B magnitude, age, mass, star formation rate, and specific star formation rate (SSFR) per unit galaxy stellar mass are listed for all four tested extinction laws. Fig. 8 represents the best model corresponding to the MW extinction law.

These results confirm the previous host galaxy studies (Cucchiara et al. 2013a; de Ugarte Postigo et al. 2014; Chrimes et al. 2018) by independent observations and modeling, and adding a new piece of information about the extinction law inside the host galaxy. Our SED modeling results also constrain that SFR and mass of the host galaxy of sGRB 130603B are typical to those observed in case of other short bursts as shown in Fig. 11. However, the resulting SFR is five times higher than that obtained by Chrimes et al. (2018), using different population synthesis libraries.

4 MULTIWAVELENGTH OBSERVATIONS OF EIGHT SGRBS DURING 2012–2015

During 2012–2015, a total of 45 sGRBs were localized by several space missions. Only 23/45 of these sGRBs were seen by *Swift*-XRT. Out of those 23, only 9 were detected at optical bands, and, for 7 such events redshifts were determined. In this section, details of the prompt emission and multiband observations to detect optical afterglow and host-galaxy of eight events (sGRB 121226A, sGRB 131224A, sGRB 140606A, sGRB 140622A, sGRB 140903A, sGRB 140930B, sGRB 141212A, and sGRB 151228A) besides sGRB 130603B are discussed. Out of these eight sGRBs, three events, namely sGRB 131224A, sGRB 140606A, and sGRB 151228A, were not detected by *Swift*-XRT. However, sGRB 140606A and sGRB 151228A were seen by *Fermi*-Gamma-ray Burst Monitor (GBM) continuous Time-Tagged Event (TTE) data having detailed description in Appendix 'A'. Out of the eight sGRBs from the present sample during 2012–2015, late-time follow-up observations using GTC 10.4 m and Gemini-N 8.0 m could be obtained for 4 *Swift*-XRT localized bursts i.e. for sGRB 121226A, sGRB 140622A, sGRB 140930B, and sGRB 141212A, useful to constrain late-time afterglow emission, placing limits on possible 'kilonovae' emission and host galaxy as described in respective sections of Appendix 'A'.

The *INTEGRAL* SPI-ACS having a stable background (see Bisnovatyi-Kogan & Pozanenko 2011 and Minaev et al. 2010 for details) is particularly useful in the search for EE after the prompt emission phase of sGRBs. As a part of the present analysis, prompt emission *INTEGRAL* SPI-ACS observations of sGRB 121226A, sGRB 130603B, sGRB 140606A, sGRB 140930B, sGRB 141212A, and sGRB 151228A were analyzed and compared with other contemporaneous observations with the *Swift*-BAT and *Fermi*-GBM, when available. Details about the gamma-ray and X-ray data analysis are described in respective sub-sections of Appendix 'A'. The analysis of the sub-set of these events does not show any signature of extended emission except sGRB 121226A and their spectral and temporal properties do not differ from those seen by *Swift*-BAT. Out of the eight sGRBs, for sGRB 140606A and sGRB 151228A, the characteristic photon peak energy E_{peak} could be determined using the prompt emission *Fermi*-GBM data. These two sGRBs along with others discussed in this paper with presumed redshift values allowed us to construct the Amati diagram along with published lGRBs (see Fig. 9). Based on this diagram, nature of these four bursts (namely sGRB 140606A, sGRB 140622A, sGRB 140930B, and sGRB 151228A) are clearly categorized as short bursts.

Follow-up observations of these eight sGRBs suggest that the afterglows of these events were faint and were located either next to a bright star or embedded within the host galaxy, making the photometry complicated at the epoch of observations. Photometric results regarding the afterglow or host galaxies observed by the GTC 10.4 m and other ground-based telescopes as a part of the present analysis are tabulated in Table 5. Our optical-NIR observations indicate that for sGRB 141212A, the observed host galaxy was relatively bright and had star formation activity. Deeper GTC 10.4 m observations of the sGRB 140622A reveal that the burst could belong to a group of host-less bursts (Tunnicliffe et al. 2014). Follow-up optical observations of sGRB 140903A constrain any underlying 'kilonovae' emission down to a limiting magnitude of

Table 4. GRB 130603B host galaxy properties derived from the SED fitting using stellar population synthesis models.

Fitted parameters	Starburst model	MW model	LMC model	SMC model
χ^2/dof	12.0/11	11.1/11	11.7/11	12.2/11
Type	Sbc	Sd	Sd	Sc
$E(B-V)$, mag	0.05	0.20	0.20	0.00
M_B, mag	-20.05 (±0.07)	-20.86 (±0.07)	-20.06 (±0.07)	-20.83 (±0.07)
Age, Gyr	$0.58^{+0.60}_{-0.42}$	$0.72^{+0.84}_{-0.55}$	$3.75^{+0.80}_{-2.25}$	$7.50^{+0.44}_{-5.82}$
Mass, ($\times 10^{10}$) $M_\odot$	$1.4^{+0.4}_{-0.1}$	$1.1^{+0.2}_{-0.7}$	$0.2^{+1.1}_{-0.1}$	$1.5^{+1.2}_{-0.9}$
SFR, $M_\odot$/yr	$8.3^{+16.8}_{-4.6}$	$5.9^{+11.9}_{-1.8}$	$7.6^{+16.4}_{-3.7}$	$8.3^{+17.2}_{-4.3}$
SSFR, ($\times 10^{-10}$) yr^{-1}	$4.6^{+15.3}_{-2.1}$	$5.3^{10.8}_{-1.0}$	$5.3^{+19.5}_{-1.1}$	$2.1^{+25.3}_{-3.7}$

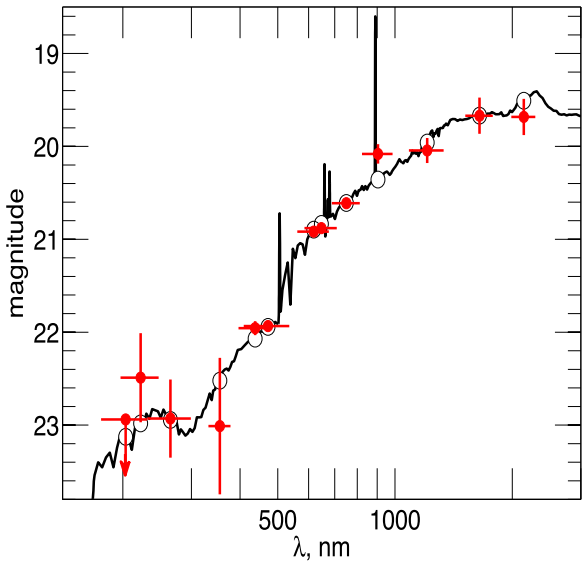

Figure 8. The SED of the host galaxy of sGRB 130603B fitted by the LEPHARE with fixed redshift $z = 0.356$. Filled red circles depict, respectively, the data points in the filters *uvw*2, *uvm*2, *uvw*1, *U*, taken from de Ugarte Postigo et al. (2014, Table 4), and *B*, *g*, *r*, R_C, *i*, *z*, *J*, *H*, K_s from original observations (see Section 2.2). Data points in *B* and R_C pass-bands were obtained using the 4K × 4K CCD Imager (Pandey et al. 2018) mounted at the axial port of the recently commissioned 3.6m DOT at Nainital, India (Kumar et al. 2018). Open circles represent model magnitudes for each filter. All magnitudes are in AB system.

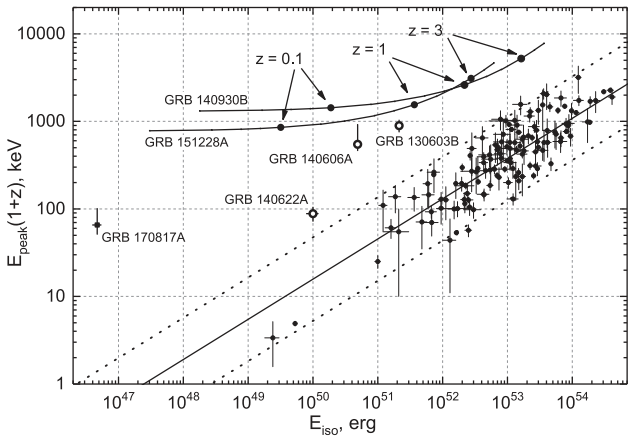

Figure 9. Amati diagram – a relation between equivalent isotropic energy emitted in the gamma-ray E_{iso} versus characteristic photon peak energy $E_{peak}(1+z)$ in the rest frame (Amati et al. 2008). The solid straight line indicates a power-law fit to the dependences for the long bursts; the dashed lines bound the 2σ correlation region. The trajectories of sGRB 140930B and sGRB 151228A are plotted as a function of the presumed redshift *z*. Open circles indicate short bursts (sGRB 140606A, sGRB 140622A, and sGRB 130603B) with measured values of E_{peak} and redshift. Parameters of sGRB 170817A/GW170817 are also overplotted for comparisons.

$R > 22$ mag at 10d after the burst. Our early- to late-time afterglow observations of sGRB 140930B using William Herschel Telescope (WHT) 4.2 m and Gemini-N 8.0 m observations along with those observed by *Swift*-XRT are able to constrain the decay nature of the burst and late time 10.4 m GTC observations places a deeper upper limit of $r \sim 24.8$ mag for any possible host galaxy. Details about observations of the afterglows, host galaxies and their data analysis, calibrations etc. of each of the eight individual bursts are described in Appendix 'A' below. A summary of the observed prompt emission and afterglow properties of all the nine sGRBs is also listed in Table 6.

5 GW170817 AND THE SAMPLE OF SGRBS

On 2017 August 17, 12:41:04.82 UT, the LIGO and Virgo interferometers detected a transient GW signal from a source named GW170817 (Abbott et al. 2017b). The *Fermi*-GBM triggered and located a short burst named sGRB 170817A (von Kienlin et al. 2017) about 1.7 s after the GW signal spatially consistent with the GW event (Blackburn et al. 2017). The error region was later followed up extensively at lower frequencies to search for the underlying 'kilonova' signature (Coulter et al. 2017; Covino et al. 2017; Cowperthwaite et al. 2017; Evans et al. 2017; Pian et al. 2017; Smartt et al. 2017; Tanvir, Levan & Gonzalez-Fernandez 2017; Troja et al. 2017). Discovery of this first GW event called GW170817/AT 2017gfo/SSS17a associated with the very nearby (host galaxy NGC 4993 at ∼40 Mpc) sGRB 170817A and the underlying bright 'kilonova' provides strong evidence favoring compact binary mergers as the progenitors for at least some of these events (see Abbott et al. 2017a,b, and references therein).

The T_{90} duration of this GW170817 connected sGRB 170817A was 0.5 ± 0.1 s (70–300 keV) having multiple emission episodes and had a relatively soft spectrum with $E_{peak} = 65^{+35}_{-14}$ keV (Goldstein al. 2017; Pozanenko et al. 2018). The burst was also detected by SPI-ACS onboard *INTEGRAL* (Savchenko et al. 2017) and morphology of the γ-ray light-curve is similar to that seen in the case of presently discussed sGRB 140930B i.e. having multiple episodes of emissions and belong to pattern-II class of bursts (Lu

Table 5. Summary of the optical photometric observations (AB-magnitudes) of the afterglows of the eight sGRBs (2012–2015) and their host galaxies (h) using ground-based optical telescopes as a part of this study. Recently observed GW170817 using GTC 10.4 m are also appended to this table. The values of the magnitudes are in AB system (limiting magnitudes are 3σ) and no extinction corrections have been applied.

t-t0 mid(d)	exp(s)	Afterglow/ Host galaxy	Pass-band	Telescopes
		sGRB 121226A		
0.0042	5 × 19	>19	clear	0.6 m BOO-4 MET
0.0833	300 × 4	>18.8	I_c	1.04 m ST ARIES
0.0833	300 × 6	>19.5	R_c	1.04 m ST ARIES
0.432	75 × 2	23.65 ± 0.37	*z*	GTC 10.4 m
0.441	85 × 5	24.03 ± 0.32	*i*	GTC 10.4 m
0.451	70 × 8	24.30 ± 0.30	*r*	GTC 10.4 m
53.25	50 × 31	>23.79	*z*	GTC 10.4 m
53.27	70 × 12	>24.47	*i*	GTC 10.4 m
		sGRB 131224A		
1.111	30 × 1	>18.3	*r*	GTC 10.4 m
1.113	60 × 3	>19.5	*i*	GTC 10.4 m
1.116	75 × 3	>24.3	*z*	GTC 10.4 m
7.099	5 × 4 + 10 × 1	>23.6	*i*	GTC 10.4 m
7.105	20 × 4 + 10 × 1	>22.8	*z*	GTC 10.4 m
		sGRB 140606A		
0.3315	3600	>21.7	clear	Abastumani AS-32
0.4292	4 × 30 + 3 × 120	>26.0	R_c	BTA6.0 m
0.3857	120 + 30	>24.2	*V*	BTA6.0 m
0.3893	120	>24.4	*B*	BTA6.0 m
271.642	60 × 5	>25.36	*r*	GTC 10.4 m
		sGRB 140622A		
0.0687	4320	>23.64	r	RATIR 1.5 m
0.0687	4320	>23.49	i	RATIR 1.5 m
0.0687	1836	>19.41	Z	RATIR 1.5 m
0.0687	1836	>18.73	Y	RATIR 1.5 m
0.4752	4800	>22.5	R	TShAO Ziess-1000
0.781	100 × 6 + 5 × 2	>25.8	*r*	GTC 10.4 m
		sGRB 140903A		
0.1406	100	>18.6	clear	ISON-Kislovodsk SANTEL-400A
1.0648	720	>22.0	R	Maidanak AZT-22
3.0072	900	>22.0	R	Maidanak AZT-22
4.0090	900	>22.0	R	Maidanak AZT-22
10.0500	720	>22.0	R	Maidanak AZT-22
		sGRB 140930B		
0.0291	3600	>20.4	clear	ISON-Kislovodsk, SANTEL-400A
0.0145	1200	>19.5	clear	ISON-Kislovodsk, SANTEL-400A
0.0309	2000	>19.6	clear	ISON-Krasnodar, Astrosib
0.0249	415	>16.1	clear	UAFO ORI-65
0.133	300 × 5	22.65 ± 0.09	*r*	WHT 4.2 m/ACAM
0.153	300 × 5	22.61 ± 0.06	*i*	WHT 4.2 m/ACAM
0.172	400 × 2	23.17 ± 0.12	*g*	WHT 4.2 m/ACAM
0.677	150 × 9	24.01 ± 0.04	*r*	Gemini North/GMOS-N
1.656	150 × 9	25.11 ± 0.11	*r*	Gemini North/GMOS-N
3.141	60 × 13	>24.5	*r*	GTC 10.4 m
1535.5	90 × 34	>24.75	*r*	GTC 10.4 m
		sGRB 141212A		
0.0189	60 × 10	>22.2	R	Mondy AZT33-IK
0.0363	60 × 60	22.73 ± 0.26 (h)	R	Mondy AZT33-IK
0.0783	120 × 30	22.75 ± 0.28 (h)	R	Mondy AZT33-IK
0.0573	60 × 60 + 120 × 30	22.71 ± 0.19 (h)	R	Mondy AZT33-IK

Table 5 – *continued*

t-t0 mid(d)	exp(s)	Afterglow/ Host galaxy	Pass-band	Telescopes
0.0242	60 × 5	>18.5	clear	Khureltogot ORI-40
0.0641	60 × 74	>19.9	clear	Khureltogot ORI-40
0.6814	180 × 5	22.13 ± 0.04 (h)	*i*	Gemini North/GMOS-N
1.1563	300 × 13	22.63 ± 0.18 (h)	R	TShAO Ziess-1000
1.7461	180 × 5	22.23 ± 0.04 (h)	*i*	Gemini North/GMOS-N
2.0544	120 × 57	22.76 ± 0.33 (h)	R	Mondy AZT33-IK
6.0676	120 × 85	22.86 ± 0.16 (h)	R	Mondy AZT33-IK
427.375	5 × 3 + 120 × 11	23.86 ± 0.08 (h)	*g*	GTC 10.4 m
427.385	120 × 7	22.80 ± 0.06 (h)	*r*	GTC 10.4 m
427.403	90 × 6	22.32 ± 0.05 (h)	*i*	GTC 10.4 m
		sGRB 151228A		
0.0011	60 × 3 + 20 × 2	>17.5	*R*	0.60 m T60
1.1429	5 × 60	>23.7	*i*	GTC 10.4 m
69.0036	7 × 75	>24.8	*i*	GTC 10.4 m
		sGRB 170817A/GW170817		
154.7	120 × 30	>24.0	*i*	GTC 10.4 m
536.8	120 × 10	>24.0	*i*	GTC 10.4 m

et al. 2017), suggesting a diverse set of progenitors and central engines (Dichiara et al. 2013). sGRB 170817A turned out to be the weakest detected sGRB having a soft spectrum with a thermal tail and was underluminous by a factor of ∼1000 in comparison to known sGRBs. So, observed properties like harder pulse with multiple episodes of emissions and a softer tail emission in the spectra have attracted significant attention in an effort to understand the nature of the event in terms of various physical models (Granot et al. 2017, 2018; Gottlieb, Nakar & Piran 2018; Pozanenko et al. 2018; Zhang et al. 2018). Except for resemblance with the duration T_{90}, all other observed prompt emission properties of the sGRB 170817A like the morphology of the γ-ray light-curve, $E_{\rm peak}$, $E_{\rm iso}$ etc. were outliers with the known set of sGRBs including those discussed in this paper as described in Fig. 9.

sGRB 170817A counterparts at UV-optical-NIR frequencies are distinct to those expected for GRB afterglows (Piran 1999) and predominantly follow physical mechanisms suggested for underlying 'kilonova' emission (Pian et al. 2017; Tanvir et al. 2017; Troja et al. 2017) consistent with a compact binary merger origin for this event. However, contrary to red 'Kilonova' associated with the sGRB 130603B, sGRB 170817A UV-optical-NIR emission was explained well in terms of r-processed three-component subrelativistic accretion disc-powered 'kilonova' model (Villar et al. 2017a,b). In Fig. 4, the *H*-band light curve of the GW170817 counterpart (redshifted at $z = 0.36$) is compared along with 'kilonova' detection and models for the sGRB 130603B (Tanvir et al. 2013; Tanaka et al. 2014). The *H*-band redshifted light curve of the GW170817 counterpart is fainter in comparison to the corresponding *HST* detection of the 'kilonova' associated with the sGRB 130603B and exhibits distinct nature of the overall temporal decay.

Early time non-detection by the *Swift*-XRT until 9d post-burst for sGRB 170817A compared to other known cases of X-ray-detected sGRBs (Fong et al. 2017) places a constraint on the underlying emission mechanisms and supports a non-afterglow origin for the observed emission at lower frequencies. Recently, using deeper data set of other bursts, Gompertz et al. (2018) have concluded that not all sGRBs are associated with 'kilonovae' and share a diverse range of observed brightness. No detection of GW170817 like 'kilonova' for a good number of well-studied sGRBs to a deeper limit also indicate a diverse set of progenitors for some of the bursts (Gompertz et al. 2018; Rossi et al. 2019).

As a part of this study, sGRB 170817A/GW170817 was observed using GTC 10.4 m in *i*-band starting around 05:47:40 UT on 19-01-2018 for a total exposure time of 1 h (120s×30). The images were stacked and processed as per standard techniques. A 3σ upper limit of the stacked image is $i \sim 25$ mag whereas at the location of the optical transient (see Fig. 10 and Table 5), a rather shallow value of $i \sim 23.5$ mag was estimated due to contamination of the host. As a part of the present analysis, second epoch of GTC 10.4 m observations of the host galaxy NGC 4993 were also on 06-02-2019 around 5:10:00 UT in the *i* band (120s×30) and after image subtraction a deeper limit of $i \sim 24$ mag was estimated at the location of the GW170817. This observed limiting magnitude (∼154.7d post-burst) at the location of the optical transient is in agreement with the extrapolated at contemporaneous epochs by Margutti et al. (2018) and thus supports a non-thermal origin of the emission at the epoch of our observations. On the other hand, detections of the sGRB 170817A/GW170817/AT 2017gfo/SSS17a at X-ray (Troja et al. 2017) and VLA radio frequencies (Alexander et al. 2017) ∼9d to 160d post-burst exhibit rising light curves at both X-ray and radio frequencies and are broadly consistent with non-thermal collimated emission viewed off-axis or structured outflow (Granot et al. 2002, 2017; Evans et al. 2017; Fong et al. 2017; Haggard D. et al. 2017; Hallinan et al. 2017; Margutti et al. 2017; Smartt et al. 2017; Troja et al. 2017; Lazzati et al. 2018). However, Xie, Zrake & MacFadyen (2018) and Lyman et al. (2018) have found that the late-time multiband data of the sGRB 170817A is well explained by both narrow and wide engine mild-relativistic models, though, early time non-detection at X-ray frequencies disfavors wide engine model. So, it is clear that none of the models have been able to reproduce the full set of multiband data for this nearby event.

The host galaxy SED modeling of sGRB 130603B and sGRB

Table 6. Summary of the prompt emission and afterglow properties of the nine sGRBs discussed in this paper. The symbols used in the table have their usual meanings as discussed in the main text.

sGRB	Redshift	T_{90} sec	$E_{\rm iso}$ [a] erg	$E_{\rm peak}$ keV	Early first observation t-t0,mid(s)	Magnitude	Pass-band	Telescope	Afterglow detection	Host galaxy	Comments
121226A	–	1.00 ± 0.20^{a}	–	–	93	>17.5	*R*	Zadko[a]	+	>24.6(*r*)	EE
130603B	0.3564 ± 0.0002^{a}	0.18 ± 0.02^{b}	$(2.1 \pm 0.2) \times 10^{51\ b}$	660 ± 100^{a}	137	>19.6	*white*	UVOT[b]	+	$22.13 \pm 0.05(r)$	KN
131224A	–	0.8^{c}	–	–	44	>15.5	*white*	MASTER II[c]	–	>23.6(*i*)	not a GRB
140606A	1.96 ± 0.1	0.34 ± 0.09^{d}	4.9×10^{50}	$185.13^{+126\ d}_{-28}$	143	>21.1	*white*	UVOT[d]	–	>25.3(*r*)	
140622A	0.959^{b}	0.13 ± 0.04^{e}	$(1.0 \pm 0.2) \times 10^{50}$	44 ± 8^{b}	106	>17.5	R	TAROT[e]	–	>25.8(*r*)	
140903A	0.351^{c}	0.30 ± 0.03^{f}	$(6.0 \pm 0.3) \times 10^{49\ c}$	–	152	>20.0	*white*	UVOT[f]	+	$20.58 \pm 0.09(r')^{a}$	
140930B	–	0.84 ± 0.12^{g}	–	$1302^{+2009\ c}_{-495}$	44	>16.0	*white*	MASTER II[g]	+	>25.1(*r*)	
141212A	0.596^{d}	0.30 ± 0.08^{h}	$(6.7 \pm 1.1) \times 10^{49}$	–	51	>16.8	*white*	MASTER II[h]	–	$22.80 \pm 0.06(r)$	
151228A	–	0.27 ± 0.01^{i}	–	$261.18^{+164.94\ d}_{-58.28}$	95	>17.5	R	T60	–	>24.8(*i*)	

Notes. References
Redshift: [a]Xu et al. (2012), [b]Hartoog et al. (2014), [c]Cucchiara et al. (2014), [d]Chornock et al. (2014)
T_{90}: [a]Baumgartner et al. (2012), [b]Barthelmy et al. (2013), [c]Mereghetti et al. (2013), [d]Cummings et al. (2014a), [e]Sakamoto et al. (2014b)
$E_{\rm iso}$: [a]for GRB 130603B and GRB 140622A in the range 1–10 000 keV, for other GRBs in the range 15–150 keV, [b]Frederiks (2013), [c]Troja et al. (2016)
[f]Palmer et al. (2014a), [g]Baumgartner et al. (2014), [h]Palmer et al. (2014b), [i]Barthelmy et al. (2015)
$E_{\rm peak}$: [a]Golenetskii et al. (2013), [b]Sakamoto et al. (2014b), [c]Golenetskii et al. (2014), [d]Present analysis
Early first observation: [a]Klotz et al. (2012), [b]Melandri et al. (2013), [c]Gorbovskoy et al. (2013), [d]Stroh et al. (2014a), [e]Klotz et al. (2014)
[f]Breeveld & Cummings (2014), [g]Gorbovskoy et al. (2014), [h]Gres et al. (2014).
Host galaxy: [a]Troja et al. (2016).

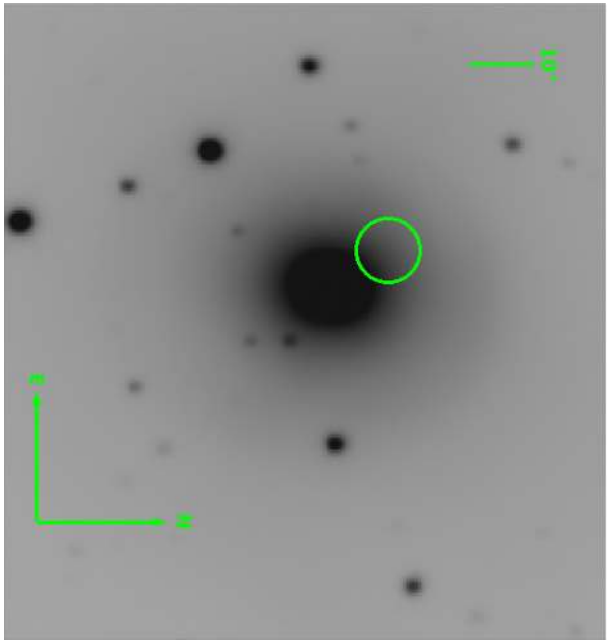

Figure 10. Finding chart of GW170817 (circle) in the stacked frame of *i*-band data obtained by the GTC 10.4 m telescope obtained ∼154.7d post-burst as a part of the present analysis.

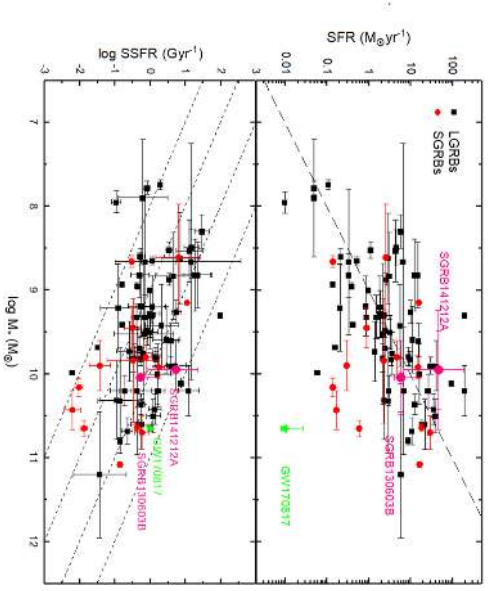

Figure 11. Plot of star formation rate versus stellar mass (top panel) and specific star formation rate versus stellar mass (bottom panel) for the known set of host galaxies of lGRBs and sGRBs. The dashed line marks a constant SFR of 1 $\rm Gyr^{-1}$ (top panel). The dashed lines mark the constant specific SFR of 0.1, 1, 10, and 100 $\rm Gyr^{-1}$ from left to right (bottom panel). The modeled values of star formation rates and mass of the hosts of sGRB 130603B and sGRB 141212A (date taken from the present analysis; Table 4 and Table A1) are plotted as pink circles. Corresponding values for the GW170817 are plotted as green star.

141212A from the present sample of bursts indicates that their respective hosts are young and bluer with moderate values of star formation activity. However, in case of sGRB 170817A, the host galaxy NGC 4993 is an old elliptical galaxy with little star formation activity and the projected offset of the burst location is rather closer to what has been seen in case of other sGRBs (Fong et al. 2017; Levan et al. 2017). Fig. 11 shows the distribution of star formation rates versus stellar mass (top panel) and specific star formation rates versus stellar mass (bottom panel) for the known set of host galaxies

of lGRBs and sGRBs (Savaglio, Glazebrook & Le Borgne 2009) and GW170817 (Blanchard et al. 2017). In Fig. 11, corresponding values for the sGRB 170817A/GW170817 clearly indicate that the star formation rate for sGRB 170817A/GW170817 host galaxy is well below from those seen in case of normal population of GRBs. Overall properties of the GRB 170817A/GW170817 and their comparison with other sGRBs indicate that we need multiwavelength observations of a significantly larger number of nearby events to explore the full diversity of 'kilonovae' and their association with sGRBs.

6 CONCLUSIONS

(i) In this work, we have analyzed and reported prompt emission data of nine short bursts including sGRB 130603B as observed by *Swift*, *INTEGRAL*, and *Fermi* observatories. The SPI-ACS *INTEGRAL* prompt emission observations of sGRB 130603B, sGRB 140930B, sGRB 141212A, and sGRB 151228A in the energy range 0.1–10 MeV do not show any EE, which is in agreement with those seen in the case of *Swift* observations. However, in case of sGRB 121226A, the EE was seen as discussed in Appendix Section A1. Using *Fermi*-GBM data, $E_{\rm peak}$ values were determined for sGRB 140606A and sGRB 151228A, and Amati diagram was constructed to establish the nature of the five sGRBs from the present sample. Also, analysis of the *INTEGRAL*/JEM-X observations indicates that sGRB 131224A may not be of a cosmological origin as discussed in the Appendix Section A2.

(ii) Multiwavelength afterglow observations for sGRB 130603B presented in this paper include the earliest ground-based optical detection and millimeter observations complementary to those published in the literature. Our *r*- and *i*-band data, together with those previously published, have helped to produce a well-sampled *r*-band light curve, and made it possible to estimate the value of pre-jet break temporal index $\alpha_1 = 0.81 \pm 0.14$ robustly. The derived values of pre- and post-jet break temporal flux decay indices along with the X-ray and optical-NIR spectral indices support the *ISM* afterglow model with cooling frequency $\nu_{\rm c}$ between optical and X-ray frequencies.

(iii) Derived values of the jet-break time and electron energy index were used to model the afterglow data of sGRB 130603B using numerical simulation-based Monte Carlo model as described in Zhang et al. (2015). Except at very early times (<1000s) and very late time (>100 000s), largely the multiband data of sGRB 130603B are explained in terms of forward shock fireball model. The derived values of microphysical parameters of the burst are better constrained than those reported in Fong et al. (2014a). The observed mm- and cm-wavelength upper limits for sGRB 130603B are also consistent with forward-shock model predictions.

(iv) In this paper, using the reported values of photometric upper limits in bluer bands (i.e. *Swift*-UVOT *u* and Gemini-N g' bands at ∼1.5d after the burst), we attempted to constrain the possible blue component of 'kilonova' emission in case of sGRB 130603B. Accordingly, the values of the ejected mass were calculated as proposed by Kasen et al. (2015) and Metzger et al. (2010) for the possible blue emission. However, the shallower observed limits at early epochs in *Swift*-UVOT *u* and Gemini-N g' bands do not provide any meaningful constraint for the blue component of 'kilonova' emission for sGRB 130603B but indicate that some of sGRBs may not have the predicted blue component.

(v) Deep afterglow observations of a further eight sGRBs using GTC 10.4 m and other telescopes reveal the nature of the decay and the complex environments of some of sGRBs not well-studied so far. In case of sGRB 140930B, our early to late-time afterglow observations using 4.2 m WHT and 8.0 m Gemini-N along with those observed by *Swift*-XRT are able to constrain the decay nature of the burst and the late-time 10.4 m GTC observations places a deeper upper limit of $r \sim 24.8$ mag for any possible host galaxy, whereas, in the case of sGRB 140622A, our optical observations using 10.4 m GTC put a deep limit of ∼25.6 mag for any afterglow or a host galaxy within XRT error-box. These deep observations by the GTC 10.4 m also indicate that sGRB 140622A could belong to the category of known host-less bursts.

(vi) Observed limiting flux values at mm- and cm-wavelengths for a set of nine sGRBs using PdBI and their comparison with published light curve of lGRB 130427A at 3 mm place constraints on the possible underlying physical mechanisms and demand for much deeper observations at these wavelengths.

(vii) Deeper optical-NIR follow-up observations of four *Swift*-XRT localized bursts sGRB 121226A, sGRB 140903A, sGRB 140930B, and sGRB 141212A using GTC 10.4 m, Gemini-N 8.0 m, and Maidanak AZT-22 1.5m upto a few days post-burst constrain for any 'kilonova' such as the one associated with the GW170817. Using prescription given in Rossi et al. (2019), comparison of rest-frame luminosity of 'kilonova' associated with GW170817 indicate that for sGRB 141212A, any such event would have been detected at the epoch of our Gemini-N 8.0 m observations. However, in cases of sGRB 121226A, sGRB 130603B, sGRB 140903A, and sGRB 140930B, the derived luminosity values were found to be dominated by afterglow i.e. brighter than the 'kilonova' associated with the GW170817.

(viii) Upper limit derived using late time (154.7d post-burst) GTC 10.4 m observations ($i \sim 23.5$ mag) of the GW170817 is in agreement with non-thermal origin of the emission as seen at other wavelengths. Comparison of prompt emission and properties of the host galaxy of the GW170817 discussed in this work point towards diverse properties of associated 'kilonovae' and in turn points towards possibly diverse classes of compact binary mergers producing normal sGRBs and those with associated 'kilonovae'.

(ix) Optical-NIR photometry of the host galaxy of sGRB 130603B was independently modeled using LEPHARE software. The modeling results support the MW Galaxy model with a moderate value of the star formation activity in the host galaxy. We also conclude that the SFR and mass of the host galaxy are typical of those seen in case of other GRBs. The host galaxy modeling of the sGRB 141212A indicates that the host is a MW type of Sc galaxy with a moderate value of star formation.

(x) Our observations and analysis of the eight sGRBs and sGRB 170817A/GW170817 (Tables 5 and 6) demand for systematically deeper and more prompt multiwavelength observations of many of these events to detect the afterglow or to constrain the possible associated 'kilonovae', host galaxies, and their properties in more detail. In the future, *JWST* and other upcoming ground-based optical-NIR facilities like TMT and E-ELT will facilitate the study of sGRBs and GW events with unprecedented sensitivity.

ACKNOWLEDGEMENTS

Swift data/science center is thankfully acknowledged for the publically available data about GRBs. AJCT acknowledges support from the Junta de Andalucia (Project P07-TIC-03094) and support from the Spanish Ministry Projects AYA2012-39727-C03-01 and 2015-71718R. This work has been supported by the Spanish Science Ministry 'Centro de Excelencia Severo Ochoa' Program under grant SEV-2017-0709. The work is partly based on the observations made

with the Gran Telescopio Canarias (GTC), installed in the Spanish Observatorio del Roque de los Muchachos of the Instituto de Astrofisica de Canarias, in the island of La Palma Based on observations collected at the Centro Astronómico Hispano Alemán (CAHA) at Calar Alto, operated jointly by the Max-Planck-Institut for Astronomie and the Instituto de Astrofisica de Andalucia (CSIC). This research was also partially based on observations carried out at the OSN operated by CSIC. FEDER funds are acknowledged. This work is partly based on observations carried out under project numbers xa52, s14dd001, s14dd002, and s14dd006 with the IRAM NOEMA Interferometer (http://www.iram-institute.org/EN/content-page-188-7-55-188-0-0.html). S.B.P. acknowledge BRICS grant number 'DST/IMRCD/BRICS/PilotCall1/ProFCheap/2017(G)' for this work. IRAM is supported by INSU/CNRS (France), MPG (Germany), and IGN (Spain). SRO gratefully acknowledges the support of the Leverhulme Trust Early Career Fellowship. SJ acknowledges support from Korean grants NRF-2014R1A6A3A03057484 and NRF-2015R1D1A4A01020961. E.S. acknowledges assistance from the Scientific and Technological Research Council of Turkey (TUBITAK) through project 112T224. We thank TUBITAK for a partial support in using T100 telescope with project number 10CT100-95. S.B.P. acknowledge discussions with Dr. Masaomi Tanaka on kilonovae and related science. A.S.P acknowledges partial support grants RFBR 17-02-01388, 17-51-44018, and 17-52-80139. E.D.M., A.A.V., and P.Yu.M. are grateful to RSCF grant 18-12-00522 for support. B.-B.Z. acknowledges support from National Thousand Young Talents program of China and National Key Research and Development Program of China (2018YFA0404204). R.Ya.I. is grateful for partial support by the grant RUSTAVELI/FR/379/6-300/14. We thank the RATIR project team and the staff of the Observatorio Astronómico Nacional on Sierra San Pedro Mártir. RATIR is a collaboration between the University of California, the Universidad Nacional Autonóma de México, NASA Goddard Space Flight Center, and Arizona State University, benefiting from the loan of an H2RG detector and hardware and software support from Teledyne Scientific and Imaging. RATIR, the automation of the Harold L. Johnson Telescope of the Observatorio Astronomico Nacional on Sierra San Pedro Martir, and the operation of both are funded through NASA grants NNX09AH71G, NNX09AT02G, NNX10AI27G, and NNX12AE66G, CONACyT grants INFR-2009-01-122785 and CB-2008-101958, UNAM PAPIIT grant IN113810, and UC MEXUS-CONACyT grant CN 09-283. R.S.R. acknowledges support from ASI (Italian Space Agency) through the Contract No. 2015-046-R.0 and from European Union Horizon 2020 Programme under the AHEAD project (grant agreement No. 654215). SJ acknowledges the support of the Korea Basic Science Research Program through NRF-2015R1D1A4A01020961. Mondy observations were performed with budgetary funding of Basic Research program II.16 and the data were obtained using the equipment of Center for Common Use 'Angara' (http://ckp-rf.ru/ckp/3056/). We are also thankful to I. Márquez for useful discussions.

REFERENCES

Abbott B. P. et al., 2017a, ApJ, 848, L12
Abbott B. P. et al., 2017b, Phys. Rev. Lett., 161101, 119
Alard C., Lupton R. H., 1998, ApJ, 503, 325
Albert A. et al., 2017, ApJ, 850, L35
Alexander K. D. et al., 2017, ApJ, 848, 69
Amati L., Guidorzi C., Frontera F., Della Valle M., Finelli F., Landi R., Montanari E., 2008, MNRAS, 391, 577
Arnouts S., Cristiani S., Moscardini L., Matarrese S., Lucchin F., Fontana A., Giallongo E., 1999, MNRAS, 310, 540
Barkov M. V., Pozanenko A. S., 2011, MNRAS, 417, 2161
Barnes J., Kasen D., 2013, ApJ, 775, 18
Barthelmy S. D. et al., 2013, GCN Circular 14741
Barthelmy S. D. et al., 2015, GCN Circular 18754
Baumgartner W. H. et al., 2012, GCN Circular 14111
Baumgartner W. H. et al., 2014, GCN Circular 16870
Berger E., 2010, ApJ, 722, 1946
Berger E., 2014, ARA&A, 52, 43
Berger E., Fong W., Chornock R., 2013, ApJ, 774, 23
Beuermann K. et al., 1999, A&A, 352, L26
Bhatt V. K., Pandey S. B., Kumar B., 2012, GCN Circular 14109
Bildsten L., 2000, AIPC, 522, 359
Bisnovatyi-Kogan G. S., Pozanenko A. S., 2011, Astrophys. Space Sci., 332, 57
Bissaldi E., Zhang B. B., Veres P., 2015, GCN Circular 18736
Blackburn L. et al., 2017, GCN Circular 21506
Blanchard P. K. et al., 2017, ApJ, 848, L22
Blandford R. D., Znajek R. L., 1977, MNRAS, 179, 433
Bloom J. S., Kulkarni S. R., Djorgovski S. G., 2002, AJ, 123, 1111
Breeveld A.A., Cummings J. R., 2014, GCN Circular 16772
Breeveld A. A., De Pasquale M., 2013, GCN Circular 15615
Breeveld A. A., De Pasquale M., 2014, GCN Circular 16869
Breeveld A. A., Krimm H. A., 2012, GCN Circular 14113
Bromberg O., Nakar E., Piran T., Sari R., 2013, ApJ, 764, 179
Bulla M. et al., 2019, Nat. Astron., 3, 99
Burrows D. N., Kennea J. A., 2014, GCN Circular 16356
Burrows D. N. et al., 2006, ApJ, 653, 468
Burrows D. N. et al., 2014, GCN Circular 16439
Butler N. et al., 2014, GCN Circular 16436
Calzetti D., Armus L., Bohlin R. C., Kinney A. L., Koornneef J., Storchi-Bergmann T., 2000, ApJ, 533, 682
Capone J. et al., 2014, GCN Circular 16769
Castro-Tirado A. J. et al., 2005, A&A, 439, L15
Castro-Tirado A. J. et al., 2012, GCN Circular 14114
Castro-Tirado A. J. et al., 2019, A&A, to submitted
Cenko S. B., Cucchiara A., Tanvir N. R., Levan A. J., Perley D. A., 2014, GCN Circular 16873
Cenko S. B., Perley D. A., 2014, GCN Circular 16770
Chernenko A., 2011, Acta Politechn., 51, 61
Chornock R., Fong W., Fox D. B., 2014, GCN Circular 17177
Chrimes A. A., Stanway E. R., Levan A. J., Davies L. J. M., Angus C. R., Greis S. M. L., 2018, MNRAS, 478, 2
Cornelisse R. et al., 2004, Nucl. Phys. B, 132, 518
Coulter D. A. et al., 2017, GCN Circular 21529
Covino S. et al., 2017, Nat. Astron., 1, 791
Cowperthwaite P. S. et al., 2017, ApJ, 848, L17
Cucchiara A., Perley D., Cenko S. B., 2013, GCN Circular 14748
Cucchiara A. et al., 2013a, ApJ, 777, 94
Cucchiara A. et al., 2014, GCN Circular 16774
Cummings J. R. et al., 2014a, GCN Circular 16354
Cummings J. R. et al., 2014b, GCN Circular 16763
D'Avanzo P. et al., 2014, MNRAS, 442, 2342
De Pasquale M., Maselli A., Cummings J. R., 2014a, GCN Circular 16767
De Pasquale M. et al., 2014b, GCN Circular 16857
Desai D., Metzger B. D., Foucart F., 2018, MNRAS, preprint (arXiv:1812.04641)
de Ugarte Postigo A. et al., 2012, A&A, 538, A44
de Ugarte Postigo A. et al., 2013, GCN Circular 14743
d e Ugarte Postigo A. et al., 2014, A&A, 563, A62
Dichiara S., Guidorzi C., Frontera F., Amati L., 2013, ApJ, 777, 132
Dichiara S., Guidorzi C., Japelj J., 2014, GCN Circular 16781
D'Elia V. et al., 2014, GCN Circular 16433
Eichler D., Livio M., Piran T., Schramm D. N., 1989, Nature, 340, 126
Evans P. A. et al., 2017, Science, 358, 1565
Fan Y.-Z., Yu Y.-W., Xu D., Jin Z.-P., Wu X.-F., Wei D.-M., Zhang B., 2013, ApJ, 779, L25

Fernandez R., Metzger B. D., 2016, Annu. Rev. Nucl. Part. Sci., 66, 23
Feroz F., Hobson M. P., Bridges M., 2009, MNRAS, 398, 1601
Fioc M., Rocca-Volmerange B., 1997, A&A, 326, 950
Fitzpatrick E. L., 1986, AJ, 92, 1068
Foley R. J., Chornock R., Fong W., Berger E., Jha S., 2013, GCN Circular 14745
Fong W., 2014a, GCN Circular 16777
Fong W., Calkins M., Berger E., 2014b, GCN Circular 16863
Fong W., Zauderer B. A., Berger E., 2014c, GCN Circular 14126
Fong W. et al., 2013, ApJ, 769, 56
Fong W. et al., 2014a, ApJ, 780, 118
Fong W. et al., 2016, ApJ, 833, 151
Fong W. et al., 2017, ApJ, 848, L23
Fox D. B., Cummings J. R., 2014, GCN Circular 16766
Frederiks D., 2013, GCN Circular 14772
Fujiwara T. et al., 2014, GCN Circular 17160
Furchter A. S., 2014, GCN Circular 16776
Gal R. R. et al., 2003, AJ, 125, 2064
Gehrels N., Ramirez-Ruiz E., Fox D. B., 2009, ARA&A, 47, 567
Gehrels N. et al., 2005, Nature, 437, 851
Gehrels N. et al., 2006, Nature, 444, 1044
Gibson S. L., Wynn G. A., Gompertz B. P., O'Brien P. T., 2017, MNRAS, 470, 4925
Goldstein A. et al., 2017, ApJ, 848, L14
Golenetskii S. et al., 2013, GCN Circular 14771
Golenetskii S. et al., 2014, GCN Circular 16868
Gompertz B. P., Page K. L., De Pasquale M., 2013, GCN Circular 15610
Gompertz B. P. et al., 2018, ApJ, 860, 62
Gorbovskoy E. et al., 2013, GCN Circular 15608
Gorbovskoy E. et al., 2014, GCN Circular 16875
Gorosabel J., Hellmich S., Mottola S., 2014, GCN Circular 16860
Gottlieb O., Nakar E., Piran T., 2018, MNRAS, 473, 576
Graham J., Nicuesa Guelbenzu A., Bolmer J., Greiner J., 2014, GCN Circular 16872
Granot J., Gottlieb O., Piran T. et al., 2018, ApJ, 867, 18
Granot J., Guetta D., Gill R., 2017, ApJ, 850, L24
Granot J., Panaitescu A., Kumar P., Woosley S. E., 2002, ApJ, 570, L61
Gres O. et al., 2014, GCN, 17162, 1
Guilloteau S. et al., 1992, A&A, 262, 624
Guziy S. et al., 2012, GCN Circular 14106
Haggard D., Nynka M., Ruan J. J., Kalogera V., Cenko S. B., Evans P., Kennea J. A., 2017, ApJ, 848, L25
Hakkila J., Preece R. D., 2014, ApJ, 783, 88
Hallinan G. et al., 2017, Science, 358, 1579
Hartoog O. E., Malesani D., Sanchez-Ramirez R., de Ugarte Postigo A., Levan A. J., Fynbo J. P. U., Vreeswijk P. M., Kaper L., 2014, GCN, 16437, 1
Hotokezaka K., Kyutoku K., Tanaka M., Kiuchi K., Sekiguchi Y., Shibata M., Wanajo S., 2013, ApJ, 778, L16
Ilbert O. et al., 2006, A&A, 457, 841
Just O., Bauswein A., Ardevol Pulpillo R., Goriely S., Janka H.-T., 2015, MNRAS, 448, 541
Kann D. A. et al., 2011, ApJ, 734, 96
Kasen D., Fernández R., Metzger B. D., 2015, MNRAS, 450, 1777
Kasliwal M. M., Korobkin O., Lau R. M., Wollaeger R., Fryer C. L., 2017, ApJ, 843, L34
Kisaka S., Ioka K., 2015, ApJ, 804, L16
Klotz A., Macpherson D., Coward D., Gendre B., Boer M., Williams A., Martin R., 2012, GCN Circular 14107
Klotz A., Turpin D., Boer M., Gendre B., Siellez K., Dareli H., Bardho O., Atteia J. L., 2014, GCN Circular 16468
Koo D. C., Kron R. G., 1982, A&A, 105, 107
Kouveliotou C., Meegan C. A., Fishman G. J., Bhat N. P., Briggs M. S., Koshut T. M., Paciesas W. S., Pendleton G. N., 1993, ApJ, 413, L101
Krimm H. A., Cummings J. R., D'Elia V., Holland S. T., Page K. L., Sakamoto T., Siegel M. H., Starling R. L. C, 2012, GCN Circular 14105
Kulkarni S. R., 2005, preprint (arXiv:0510256)
Kumar B. et al., 2018, Bull. Soc. R. Sci. Liege, 87, 29
Kumar P., Zhang B., 2015, Phys. Rep., 561, 1
Lamb G. P., Kobayashi S., 2018, MNRAS, 478, 733
Lattimer J. M., Schramm D. N., 1974, ApJ, 192, L145
Lazzati D., Perna R., Morsony B. J., Lopez-Camara D., Cantiello M., Ciolfi R., Giacomazzo B., Workman J. C., 2018, Phys. Rev. Lett., 120, 241103
Lee W. H., Ramirez-Ruiz E., 2007, New J. Phys., 9, 17
Levan A. J., Cenko S. B., Cucchiara A., Perley D. A., 2014, GCN Circular 16784
Levan A. J. et al., 2017, ApJ, 848, L28
Lewin W. H. G., van Paradijs J., Taam R. E., 1995, X-ray binaries. p. 175
Li L.-X., Paczyński B., 1998, ApJ, 507, L59
Littlejohns O. M. et al., 2012, GCN Circular 14112
Lloyd-Ronning N. M., Zhang B., 2004, ApJ, 613, 477
Loeb A., 2016, ApJ, 819, L21
Lu R. J., Du S. S., Cheng J. G., Lü H.-J., Zhang H.-M., Lan L., Liang E.-W., 2017, ApJ, preprint (arXiv:1710:06979v1)
Lyman J. D. et al., 2018, Nat. Astron., 2, 751
Malesani D., D'Avanzo P., D'Elia V., Vergani S. D., Andreuzzi G., Garcia A., Escudero G., Bonomo A., 2014, GCN Circular 17170
Malesani D., D'Avanzo P., Melandri A., Covino S., Fiorenzano A., di Fabrizio L., Andreuzzi G., 2013, GCN Circular 14139
Margutti R. et al., 2017, ApJ, 848, L20
Margutti R. et al., 2018, ApJ, 856, L18
Marshall F. E., D'Elia V., 2014, GCN Circular 16446
Massarotti M., Iovino A., Buzzoni A., Valls-Gabaud D., 2001, A&A, 380, 425
Mazets E. P. et al., 1981, Astrophysics and Space Science, 80, 3
Melandri A. et al., 2013, GCN Circular 14735
Mereghetti S., Gotz D., Bozzo E., Ferrigno C., Malishev D., Borkowski J., 2013, GCN Circular 15607
Metzger B. D., Berger E., 2012, ApJ, 746, 48
Metzger B. D., Fernández R., 2014, MNRAS, 441, 3444
Metzger B. D., Piro A. L., 2014, MNRAS, 439, 3916
Metzger B. D., Piro A. L., Quataert E., 2008, MNRAS, 390, 781
Metzger B. D. et al., 2010, MNRAS, 406, 2650
Minaev P., Pozanenko A., Molkov S., 2018, Int. J. Mod. Phys. D, 27, 1844013
Minaev P. Y., Grebenev S. A., Pozanenko A. S., Molkov S. V., Frederiks D. D., Golenetskii S. V., 2012, Astron. Lett., 38, 613
Minaev P. Y., Pozanenko A. S., 2017, Astron. Lett., 43, 1
Minaev P. Y., Pozanenko A. S., Loznikov V. M., 2010, Astron. Lett., 36, 707
Minaev P. Y., Pozanenko A. S., Molkov S. V., Grebenev S. A., 2014, Astron. Lett., 40, 235
Minaev P. Yu., Pozanenko A. S., 2019, under preperation
Mooley K. P. et al., 2018, Nature, 554, 207
Moskvitin A. S. et al., 2014, GCN Circular 16411
Nakar E., 2007, Phys. Rep., 442, 166
Narayan R., Paczynski B., Piran T., 1992, ApJ, 395, L83
Nayana A. J., Chandra P., 2014, GCN Circular 16815
Nesterov N. S., Volvach A. E., Strepka I. D., 2000, Astron. Lett., 26, 204
Nicuesa Guelbenzu A. et al., 2012, A&A, 548, A101
Nissanke S., Mansi K., Georgieva A., 2013, ApJ, 767, 124
Norris J., Gehrels N., Barthelmy S. D., Sakamoto T., 2013, GCN Circular 14746
Oates S. R., Ukwatta T. N., 2014, GCN Circular 17180
Page K. L., 2015, GCN Circular 18772
Palmer D. M. et al., 2014a, GCN Circular 17175
Palmer D. M. et al., 2014b, GCN Circular 16768
Pandey S. B., Yadav R. K. S., Nanjappa N., Yadav S., Reddy B. K., Sahu S., Srinivasan R., 2018, Bull. Soc. R. Sci. Liege, 87, 42
Perley D. A., Jencson J., 2014, GCN Circular 16867
Perley D. A. et al., 2009, ApJ, 696, 1871
Perley D. A. et al., 2014, ApJ, 781, 37
Pian E. et al., 2017, Nature, 551, 67
Piran T., 1999, Phys. Rep., 314, 575
Piran T., Nakar E., Rosswog S., 2013, MNRAS, 430, 2121
Polyakov K., Pozanenko A., Volnova A., Molotov I., 2014, GCN Circular 16862

Pozanenko A., Volnova A., Polyakov N., Romas E., Molotov I., 2014, GCN Circular 16779
Pozanenko A. S. et al., 2018, ApJ, 852, L30
Prevot M. L., Lequeux J., Maurice E., Prevot L., Rocca-Volmerange B., 1984, A&A, 132, 389
Radice D., Perego A., Hotokezaka K., Fromm S. A., Bernuzzi S., Roberts L. F., 2018, ApJ, preprint (arXiv:1809.1161)
Rhoads J. E., 1999, ApJ, 525, 737
Rossi A. et al., 2019, MNRAS, preprint (arXiv:1901.05792V1)
Rosswog S., 2005, ApJ, 634, 1202
Rosswog S., Korobkin O., Arcones A., Thielemann F.-K., Piran T., 2014, MNRAS, 439, 744
Rowlinson A., O'Brien P. T., Metzger B. D., Tanvir N. R., Levan A. J., 2013, MNRAS, 430, 1061
Ryan G., van Eerten H., MacFadyen A., Zhang B.-B., 2015, ApJ, 799, 3
Sakamoto T., Norris J., Barthelmy S. D., 2014a, GCN Circular 16771
Sakamoto T. et al., 2014b, GCN Circular 16438
Salvaterra R., Devecchi B., Colpi M., DÁvanzo P., 2010, MNRAS, 406, 1248
Sari R., Piran T., Halpern J. P., 1999, ApJ, 519, L17
Sari R., Piran T., Narayan R., 1998, ApJ, 497, L17
Savaglio S., Glazebrook K., Le Borgne D., 2009, ApJ, 691, 182
Savchenko V. et al., 2017, ApJ, 848, L15
Schady P. et al., 2007, MNRAS, 377, 273
Schady P. et al., 2010, MNRAS, 401, 2773
Schwarz U. J., 1978, A&A, 65, 345
Seaton M. J., 1979, MNRAS, 187, 73
Serino M. et al., 2014, GCN Circular 16778
Shibata M., Taniguchi K., 2011, Living Rev. Relat., 14, 6
Siegel D. M., Ciolfi R., 2016a, ApJ, 819, 14
Siegel D. M., Ciolfi R., 2016b, ApJ, 819, 14
Smartt S. J. et al., 2017, Nature, 551, 75
Sonbas E., Parmaksizoglu M., Guver T., Gogus E., Dindar M., Kirbiyik H., 2015, GCN Circular 18746
Stroh M. C., Kennea J. A., Gehrels N., 2014a, GCN Circular 16357
Stroh M. C. et al., 2014b, GCN Circular 16353
Sánchez-Ramírez R. et al., 2013, GCN Circular 14747
Tanaka M., 2016, Adv. Astron., 6341974, 1Available at: http://th.nao.ac.jp/MEMBER/tanaka/tanaka16.pdf
Tanaka M., Hotokezaka K., 2013, ApJ, 775, 113
Tanaka M., Hotokezaka K., Kyutoku K., Wanajo S., Kiuchi K., Sekiguchi Y., Shibata M., 2014, ApJ, 780, 31
Tanga M., Delvaux C., Greiner J., 2014, GCN Circular 16435
Tanvir N. R., Levan A. J., Fraser M., 2014, GCN Circular 16861
Tanvir N. R., Levan A. J., Fruchter A. S., Hjorth J., Hounsell R. A., Wiersema K., Tunnicliffe R. L., 2013, Nature, 500, 547
Tanvir N. R. et al., 2017, ApJ, 848, L27
Troja E., King A. R., O'Brien P. T., Lyons N., Cusumano G., 2008, MNRAS, 385, L10
Troja E., Rosswog S., Gehrels N., 2010, ApJ, 723, 1711
Troja E. et al., 2007, ApJ, 665, 599
Troja E. et al., 2016, ApJ, 827, 102
Troja E. et al., 2017, Nature, 551, 71
Troja E. et al., 2018, Nat. Commun., 9, 4089
Tunnicliffe R. L. et al., 2014, MNRAS, 437, 1495
Ukwatta T. N., Barthelmy S. D., Beardmore A. P., 2014, GCN Circular 17158
Ukwatta T. N., Barthelmy S. D., Cummings J. R., 2015, GCN Circular 18731
Usov V. V., 1992, Nature, 357, 472
van Eerten H. J., MacFadyen A. I., 2012, ApJ, 747, 30
Vigano D., Mereghetti S., 2009, Proceedings of The Extreme sky: Sampling the Universe above 10 keV, held in Otranto (Lecce, Italy) on 2009 October 13-17. preprint (arXiv:0912.5329)
Villar V. A., Berger E., Metzger B. D., Guillochon J., 2017b, ApJ, 849, 70
Villar V. A. et al., 2017a, ApJ, 851, 21
Villata M. et al., 2006, A&A, 453, 817
Volnova A., Inasaridze R., Kvaratskhelia O., Ayvazian V., Krugly Yu., Molotov I., Pozanenko A., 2014, GCN Circular 16371
von Kienlin A., Meegan C., Goldstein A., 2017, GCN Circular 21520
Wang X. G. et al., 2015, ApJS, 219, 9
Xie X., Zrake J., MacFadyen A., 2018, ApJ, 863, 58
Xu D., Geier S., Malesani D., Fynbo J. P. U., Harmanen J., Levan A. J., Kakobsson P., 2014a, GCN Circular 16783
Xu D., Niu H.-B., Yang T.-Z., Esamdin A., Ma L., 2014b, GCN Circular 16359
Xu D. et al., 2012, GCN Circular 14110
Xu D. et al., 2013, GCN Circular 14757
Yang B., Zin Z.-P., Li X. et al., 2015, NatureCo, 6, 7323
Zhang B., Meszaros P., 2011, ApJ, 552, L35
Zhang B., Mészáros P., 2001, ApJ, 552, L35
Zhang B.-B., Liang E.-W., Zhang B., 2007, ApJ, 666, 1002
Zhang B.-B., van Eerten H., Burrows D. N., Ryan G. S., Evans P. A., Racusin J. L., Troja E., MacFadyen A., 2015, ApJ, 806, 15
Zhang B.-B. et al., 2018, Nat. Commun., 9, 447
Zhang B. et al., 2009, ApJ, 703, 1696
Zheng W., Filippenko A. V., Morgan A., Cenko S. B., 2014, GCN Circular 16441
Zhi-Ping J. et al., 2016, Nat. Commun., 7, 12898

APPENDIX A: MULTIWAVELENGTH OBSERVATIONS OF SGRBS IN 2012–2015

A1 sGRB 121226A

Swift discovered sGRB 121226A (trigger = 544027) on 2012 December 26 at 19:09:43 UT (Krimm et al. 2012), which had a duration of $T_{90} = 1.00 \pm 0.20$s and a hard spectrum, i.e. energy fluence ratio 50–100 keV/25–50 keV = 1.4, classified as a short-hard burst (Baumgartner et al. 2012). The light curve of the burst in *Swift*-BAT data has a complex structure with negligible spectral lag, which is also in good agreement with the phenomenology of short-hard bursts. The light curve of the burst in the energy range of 100–350 keV has a feature of ∼2s duration at approximately 25s after the trigger with a statistical significance of 3σ. This feature was also found in the light curve obtained by SPI-ACS *INTEGRAL* (>100 keV) at a significance of 2.5σ. The off-axis angle of the SPI-ACS detector is 58 deg and the detector has no in-flight IBAS trigger at the time of sGRB 121226A. Taking into account simultaneous detection of the *Swift*-BAT and *INTEGRAL* SPI-ACS of the feature 25s after the burst onset, we can classify it as EE. The corresponding fluence of EE component in SPI-ACS is $S_{EE} \sim 2.4 \times 10^{-7}$ erg cm^{-2} in the (75, 1000) keV range.

Starting at ∼36s, 62.8s, and 104s after the burst, respectively, the 0.6 m BOOTES-4/MET robotic telescope at the Lijiang Astronomical Observatory (China), 1.0m Zadko robotic telescope located at the observatory at Gingin, Australia, and *Swift*-UVOT responded automatically to the trigger and did not find any optical afterglow down to a limiting magnitude of 19–20 mag (Breeveld & Krimm 2012; Guziy et al. 2012; Klotz et al. 2012). Ground-based optical follow-up observations taken with 1.04m ST at ARIES Nainital ∼2 h (Bhatt, Pandey & Kumar 2012) to 11.5 h (Xu et al. 2012) after the burst did not detect any optical source at the XRT location (Littlejohns et al. 2012). However, GTC 10.4 m multiband observations taken 10.2–10.8 h post-burst (Castro-Tirado et al. 2012) show a faint optical source consistent with the XRT position. The finding chart locating the XRT error circle is shown in Fig. A1 based on the data taken by the GTC 10.4 m as a part of the present analysis. Magnitudes of the optical source detected by the GTC 10.4 m in the *r*, *i*, *z* bands are reported in Table 5. Observations at the same location using the 3.6 m TNG ∼15.4d after the burst also detect an object (Malesani et al. 2012), which did not appear to have faded

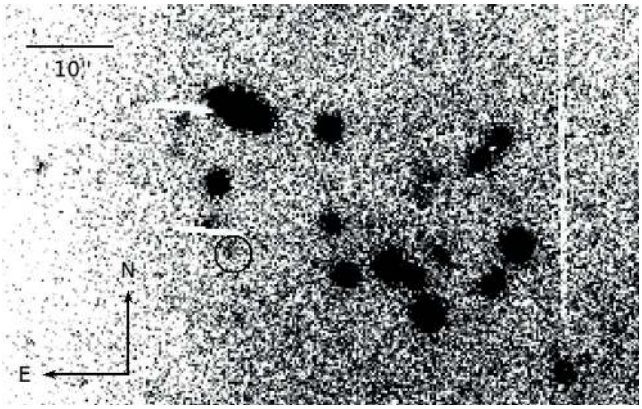

Figure A1. Finding chart of sGRB 121226A in the stacked frame of *r*-band data obtained by the GTC 10.4 m telescope. The optical afterglow candidate within the XRT error box reported in Castro-Tirado et al. (2012) is circled in the chart.

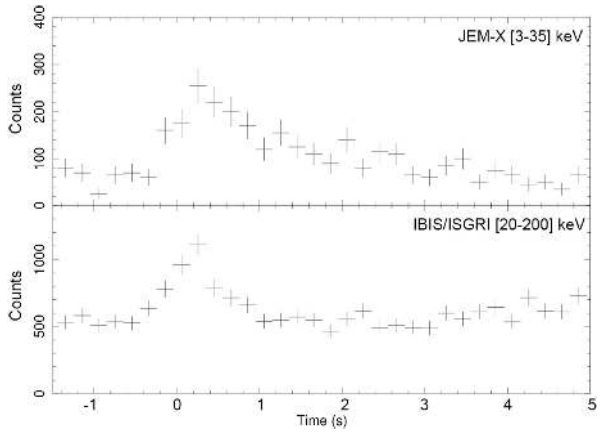

Figure A2. Light curve of sGRB 131224A obtained by JEM-X (top) and IBIS/ISGRI (bottom) onboard the *INTEGRAL* observatory with time resolution of 0.2 s.

in comparison to the detection in the *r* band taken much earlier by the 10.4 m GTC. However, the $(r-i)$ and $(z-r)$ colors of the 10.4 m GTC data are similar to those of other optical afterglows, though with large photometric errors. Our follow-up observations by the 10.4 m GTC taken around 53d post-burst in i (>24.5 mag) and z (>23.8 mag) pass-bands place deep limits for any possible host galaxy or possible underlying 'kilonova' emission in the observed pass-bands. However, the 10.4 m GTC multiband data from the present analysis, together with those observed by Malesani et al. (2012), do not firmly establish afterglow decay nature of the optical source coincident with the *Swift*-XRT (Littlejohns et al. 2012) and VLA (Fong et al. 2014c) detections. Considering that the optical source is not the host galaxy, flatter behaviour of the source between 0.5d and 15.4d post-burst has a luminosity of $L_r < 1.2 \times 10^{27}$ erg s^{-1} Hz^{-1} for an assumed redshift $z \sim 0.5$. This luminosity corresponds to 5 times brighter than the rest-frame luminosity of any possible GW170817 like 'kilonova' at similar epochs and indicates, infered value of luminosity to be afterglow dominated as seen in case of some of the sGRBs (Rossi et al. 2019). It is also notable that the *Swift*-XRT spectral analysis favors a higher Galactic absorption column density towards the burst direction (Littlejohns et al. 2012) having a steeper photon index. Further deeper observations would be required to look for any possible blue dwarf galaxy within the XRT error circle.

A2 sGRB 131224A

sGRB 131224A was discovered on 2013 December 24 at 16:54:37 UT by the Imager on Board of the *INTEGRAL* Satellite (IBIS/ISGRI) with a fluence in the energy range 20–200 keV of about $\sim 3 \times 10^{-8}$ erg cm^{-2}s^{-1} and duration of T_{90} ~0.8s (Mereghetti et al. 2013). The burst position is 2.7 deg off-axis and was also found by the Joint European X-Ray Monitor (JEM-X), X-ray telescope onboard *INTEGRAL*. The refined coordinates (J2000) are: RA = 296.821 deg, Dec. = + 31.663 deg with an uncertainty of 1 arcmin (90 per cent c.l.). The burst is located (in projection) in the Galactic plane. Spectral lag between the light curves in energy ranges 3–35 keV and 20–200 keV is negligible. The burst consists of a single FRED pulse in the 3–35 keV energy range; emission is visible up to 4s after the trigger and nearly symmetric in the hard IBIS/ISGRI channels as derived in the analysis presented in this paper (see Fig. A2). Further, we analyzed *Fermi*/GBM data and found that sGRB 131224A was within the field of view but didn't trigger *Fermi*/GBM. In the temporal analysis, we found nothing significant in the *Fermi* daily Time-Tagged Event (TTE) data. Optical observations of the *INTEGRAL* error-box by the MASTER-II robotic telescope starting ~39s after the burst trigger do not reveal any counterpart down to a limiting magnitude of ~15.5 mag (Gorbovskoy et al. 2013). *Swift*-XRT and UVOT observations starting around 2.9h after the burst do not reveal any X-ray counterpart down to a limiting flux of $\sim 1.4 \times 10^{-13}$ erg cm^{-2}s^{-1} (Gompertz, Page & De Pasquale 2013) or to a limiting magnitude of ~21.1 mag in the UVOT *u*-band (Breeveld & De Pasquale 2013), consistent with those seen in the case of other sGRBs.

It could also be discussed whether the event 131224A genuinely is a GRB event. The burst energy and morphology is very similar to type-I X-ray bursts that are thermonuclear flashes on the surfaces of weakly magnetic accreting neutron stars in low-mass X-ray binaries (LMXBs; for reviews see e.g. Lewin, van Paradijs & Taam 1995; Bildsten 2000). The burst is unusually soft for a short GRB and is not detected above 70 keV. The duration of the event in the soft (3–20 keV) energy band is 10s longer than in the hard (20–70 keV) energy band. The burst came from the direction of the Galactic plane, where the greatest number of known LMXBs are located. If the event is a type-I X-ray burst and taking into account no detection of any persistent X-ray emission in the follow-up XRT observation then this source is a new member of the rare class of X-ray bursters with very low ($<10^{35}$ erg s^{-1}) luminosity, the so-called 'burst-only' sources (see e.g. Cornelisse et al. 2004 and references therein).

Deeper observations of this burst were performed under our program using the 10.4 m GTC starting 1.11d and around 7d after the burst in i and z filters. Within the JEM-X *INTEGRAL* error-box, no new fading source was revealed down to a limiting magnitude of ~23.6 mag in the i band. The photometric results based on our analysis of the GTC data are tabulated in Table 5.

A3 sGRB 140606A

Swift discovered sGRB 140606A (trigger = 600951) on 2014 June 6 at 10:58:13 UT, which had a duration of $T_{90} = 0.34 \pm 0.09$ s (Cummings et al. 2014a; Stroh et al. 2014b). The time-averaged spectrum from T-0.04 to T + 0.35 is best fit by a simple power-law model. The burst is not visible in the soft energy channel

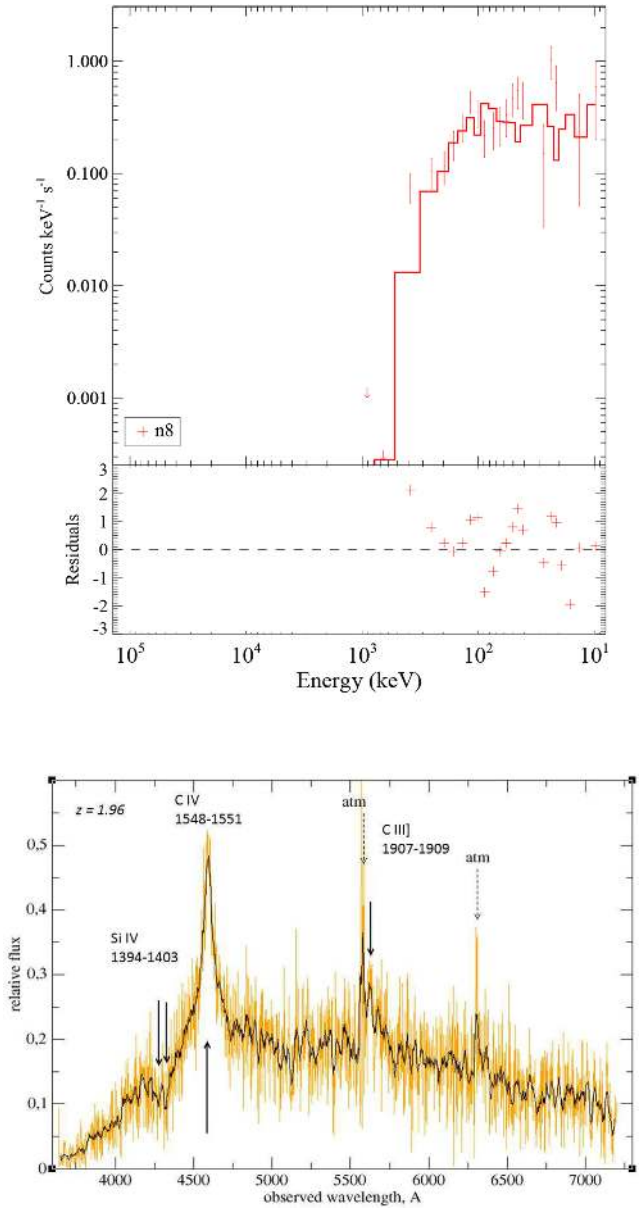

Figure A3. The best-fitting model of the prompt emission spectra of the *Fermi*/GBM (top panel) data of sGRB 140606A. The 6.0 m BTA (+SCORPIO) spectrum (4 × 900s) taken on 2014 June 7 of the new QSO (RA = $13^h27^m07.9^s$, Dec.= + 37°37′10.8″ discovered within the sGRB 140606A BAT error box showing the typical QSO emission lines at a redshift $z = 1.96 \pm 0.1$ (bottom panel).

(15–25 keV) and has negligible spectral lag. This confirms the short nature of the burst. *Fermi*/GBM data of the sGRB 140606A show that the burst was seen within the field of view but didn't trigger *Fermi*/GBM. However, significant gamma-ray emission in the *Fermi* Daily continuous Time-Tagged Event (TTE) data archive. We fit the spectrum of NaI n4 between T0−0.04 and T0+0.8s and found that cutoff-PL model is the best fit to the data. The low-energy photon index $= 0.82^{+1.34}_{-0.97}$ and $E_{peak} = 185.13^{+126}_{-28}$ keV. The corresponding GBM flux is $\sim 6.0 \times 10^{-7}$ erg cm^{-2} s^{-1} in 1–10^4 keV. The spectral fitting plot with cutoff-PL model is shown in Fig. A3 (top panel). The burst was detected by IBAS in SPI-ACS *INTEGRAL* (off-axis angle is 40 deg) as a 0.25 s single pulse and we do not detect EE (for details of SPI-ACS data analysis, see Minaev et al. 2010). At a time scale of 50s, the upper limit on EE activity in SPI-ACS for sGRB 140606A is ∼7000 counts i.e. fluence $S_{EE} \sim (7.0 \times 10^{-7}$ erg cm$^{-2})$ at the 3σ significance level in the (75, 1000) keV range.

No XRT counterpart of this burst could be observed due to an observing anomaly (Burrows & Kennea 2014). *Swift* UVOT observations, starting ∼68 s after the BAT trigger, do not detect any new optical source within the error circle (Marshall & Stroh 2014) down to a limiting magnitude of ∼20 mag. Further optical observations by Xu et al. (2014b) also do not find any new optical source within the BAT error circle. Optical observations using the Abastumani AS-32 telescope starting 0.332d after the burst do not find any optical afterglow down to a limiting magnitude of ∼21.7 in a clear filter as reported by Volnova et al. (2014).

The field of sGRB 140606A was observed in *B*, *V*, and *Rc* bands with the 6 m BTA/Scorpio-I (SAO RAS, Russia) on the night of 2014 June 7. The observations started 10 h after the trigger (Moskvitin et al. 2014). The first BTA image covers 100 per cent of the BAT refined error circle. In the stacked *R*-band image we detected a few hundred objects down to the limiting magnitude $R \sim 24.1$ mag (total exposure of 150 s). The stacked image combined from all obtained frames (total exposure of 480 s) covers 14.7 square minutes, 82 per cent of the BAT circle. The limiting magnitude of this image is $R \sim 26$ mag. The field was also observed with the 10.4 m GTC/Osiris (ORM, Spain) on 2015 February 26, almost 9 months after the burst. The stacked image combined from 5 × 60 + 10 s frames in r' band covers 13.2 square minutes, 73 per cent of the BAT circle. We detected a few hundred faint objects down to the same limiting magnitude $R \sim 26$ mag. The brightest galaxies in the BAT circle are USNO 1275-0258796 and 1275-0258743 with magnitudes of about $R \approx 18$. Due to the large number of objects in the BAT circle, we cannot suggest a single candidate for the host galaxy or any possible flaring activity by an active galaxy in the observed error circle. As a part of the present analysis, mm-wavelength observations using the IRAM Plateau de Bure Interferometer for the full BAT error circle do not result any detection down to a limiting flux of 0.33 ± 0.19 mJy around 4–15d post-burst. The details of the mm observations of the sGRB 140606A taken at 86.74 GHz are tabulated in Table 2.

A blue object within the sGRB 140606A BAT error box at coordinates RA = $13^h27^m07.9^s$, Dec. = + 37°37′10.8″ (1 arcmin error) with magnitude $R = 20.60 \pm 0.04$ was found to be a quasar at $z = 1.96$ (see Fig. A3, bottom panel). The expected chance of finding a quasar within the BTA field of view is ∼0.08 (following the QSO surface number from Koo & Kron 1982) but the lack of variability between the initial BTA frame and the late-time GTC image does not support a relationship. As mentioned above, due to lack of full coverage of the BAT error circle, the chance coincidence of the QSO gamma-ray flaring with the observed sGRB 140606A cannot be established.

A4 sGRB 140622A

Swift discovered sGRB 140622A (trigger = 602278) on 2014 June 22 at 09:36:04 UT with a duration of $T_{90} = 0.13 \pm 0.04$ s (D'Elia et al. 2014; Sakamoto et al. 2014b). The mask-weighted light curve shows a weak single FRED peak with a soft spectrum, which is best fit by a black body with kT = 11.6 ± 1.8 keV, which is not typical for the class of short bursts (Sakamoto et al. 2014b). The quickly fading X-ray light curve (temporal decay index, 7.1 ± 0.9, and mostly taken in photon counting mode) does, however, appear consistent with a short burst model, and does not appear to be similar to the light curves of SGRs or other Galactic sources (Burrows et al.

2014). The burst was not detected by SPI-ACS *INTEGRAL* most probably due to the soft spectrum. The SPI-ACS *INTEGRAL* off-axis is 125 deg. The early optical observations by 0.25m TAROT (Klotz et al. 2014) ∼23.2 s post-burst, by *Swift* UVOT ∼97 s post-burst (Marshall & D'Elia 2014), and by 0.76 m KAIT ∼198 s post-burst (Zheng et al. 2014) do not reveal any optical source down to a limiting magnitude of ∼18, 21, and 19 mag, respectively. However, optical observations taken by the TSHAO Zeiss-1000 (East) telescope starting 0.475d after the burst in R_c filters with an exposure time of 60 × 60s + 5 × 240s marginally detect a source at RA = $21^h08^m41.69^s$, Dec. = $-14^o25'08.7''$ ($\pm 0.22'$) at a magnitude of 22.5 ± 0.3 mag. In the light of other non-detection to deeper limits from the data taken before and after the epoch of observations by TSHAO Zeiss-1000 (East), it seems that this marginal detection could be false one. So, an upper limit of ∼22.5 mag is reported in Table 5. The 2.2m GROND observations taken ∼252 s after the burst do not reveal any optical counterpart within the XRT error-box down to a limiting magnitude of ∼24.3 mag, however they do detect an optical source just outside the XRT error circle (Tanga, Delvaux & Greiner 2014) at a measured redshift of z ∼0.959 using VLT observations (Hartoog et al. 2014). At this redshift, the host distance from the XRT error circle would be around 21 kpc, which could easily rule out the suspected galaxy as a potential host for sGRB 140622A. The XRT error-box was also observed by the RATIR camera at the 1.5m telescope starting ∼1.2 min after the burst in several filters and no counterpart could be detected to deeper limits (Butler et al. 2014). As a part of the present analysis, mm-wavelength observations using the IRAM Plateau de Bure Interferometer for the full BAT error circle do not result any detection down to a limiting flux of −0.37 ± 0.12 mJy within a few hours post-burst. The details of mm observations of the sGRB 140622A taken at 86.74 GHz are tabulated in Table 2.

So, to search for the potential host galaxy/counterpart, we triggered our proposal on the 10.4 m GTC. The analysis of the GTC r-band data (6 × 100 + 5 × 2 s) reveal that there is no optical counterpart down to a limiting magnitude of ∼25.8 mag at around 0.78d post-burst. So, it is clear from the above observations that the host galaxy of this burst is fainter than ∼25.8 mag. It is worth mentioning that no detection of any host galaxy down to a deep limit of $r \sim 25.8$ mag indicates sGRB 140622A to be a candidate belonging to the subset of other host-less events (Berger 2010; Tunnicliffe et al. 2014). The *Swift*-BAT fluence in the 15–150 keV band is $2.7 \pm 0.5 \times 10^{-08}$ erg cm^{-2} along with a < 0.3 micro-Jansky limit at optical frequencies place a very crude limit for this burst as a possible high redshift one (Berger 2010). Early epoch deeper observational limits at optical wavelengths and along with unusual *Swift*-BAT and XRT spectra (Burrows et al. 2014; Sakamoto et al. 2014b) also indicate the peculiar nature of this burst. The finding chart locating the XRT error-circle is shown in Fig. A4 based on the data taken by the GTC 10.4 m.

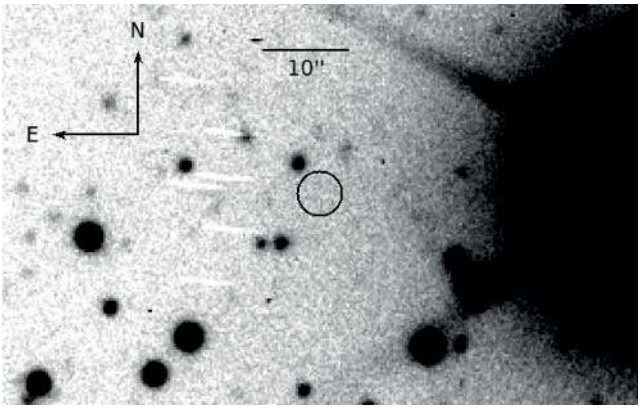

Figure A4. Finding chart of sGRB 140622A in the stacked frame of r band observed by the GTC 10.4 m telescope. The black circle is the XRT error box, having no signature of the optical afterglow down to a limiting magnitude of ∼25.8 mag ∼0.78d after the burst.

A5 sGRB 140903A

Swift- BAT triggered on a possible GRB on 2014 September 3 at 15:00:30 UT. Due to a TDRSS telemetry gap, the XRT localization was performed ∼2.5 h post-burst and ultimately the burst was found to be a duration of $T_{90} = 0.30 \pm 0.03$ s (Cummings et al. 2014b; Palmer et al. 2014b). The BAT and XRT data indicated a soft burst spectrum and an excess column density was observed (De Pasquale, Maselli & Cummings 2014a), not very common in the case of sGRBs. The time-averaged spectrum from T−0.01 to T+0.35s was best fitted by a simple power-law model. The power-law index of the time-averaged spectrum is 1.99 ± 0.12. Extended emission was not found (Sakamoto et al. 2014a; Serino et al. 2014) in the prompt emission light curve of this burst and the mask-weighted light curve shows a single FRED peak. The SPI-ACS *INTEGRAL* detector was switched off at the time of the burst. The spectral-lag analysis was performed by Sakamoto et al. (2014a) found that the spectral lag for the 50–100 keV to 100–350 keV bands is 16 ± 7ms, and 21 ± 7 ms for the 15–25 keV to 50–100 keV bands. According to Sakamoto et al. (2014a), these lag values indicate that GRB 140903A belongs to the long GRB population. This interpretation contradicts results obtained for individual pulses of BATSE bursts by Hakkila & Preece (2014). According to Hakkila & Preece (2014), short and long bursts show the same spectral evolution behaviour if spectral lag analysis is performed for individual pulses of bursts instead of analyzing the whole burst structure. Similar results were also noted by Minaev et al. (2014) in their analysis of several other *INTEGRAL* bursts. sGRB 140903A is single-pulsed and belongs to the bottom-left region of the lag duration correlation constructed for individual pulses of BATSE bursts (fig. 3 in Hakkila & Preece 2014), which means that this burst belongs to the short GRB population. A low E_{iso} value (0.04×10^{51} erg, see below) is also more common for short bursts than for long ones. Recently, Troja et al. (2016) have shown that the burst has negligible lag and other prompt emission properties are very typical of those in case of other sGRBs. It was also noticed that this burst is located within 2.5 arc-min of the center of the galaxy cluster NSC J155202 + 273349 at a photometric redshift of ∼0.295 (Gal et al. 2003; Fox & Cummings 2014). However, Troja et al. (2016) have established that the burst was not associated with the galaxy cluster.

The optical afterglow of this sGRB was discovered by the 4.3m Discovery Channel Telescope within the XRT error circle around 12 h after the burst (Capone et al. 2014; Troja et al. 2016). The optical afterglow candidate was also seen in further follow-up observations (Cenko & Perley 2014; Dichiara, Guidorzi & Japelj 2014; Xu et al. 2014a). Furchter (2014) noticed that the candidate optical afterglow was present in archival images of the Pan STARRS survey and was later suspected to be the host galaxy candidate. Troja et al. (2016) measured the redshift of the afterglow as ∼0.351, using the Gemini-N 8.0 m telescope equipped with the Gemini Multi-Object Spectrographs (GMOS) camera. The fading behaviour of the optical afterglow candidate was established in further observations by Levan et al. (2014) and Cenko et al. (2014). The radio afterglow of

the burst were also observed by JVLA at 6 GHz (Fong 2014a; Troja et al. 2016) and by GMRT at 1390 MHz (Nayana & Chandra 2014). However, mm-wavelength observations using the IRAM Plateau de Bure Interferometer at the XRT location do not result any detection down to a limiting flux of 0.12 ± 0.13 mJy within a few days post-burst. The afterglow modeling of the multiband data by Troja et al. (2016) indicates that our mm-wavelength IRAM observations were shallower in comparison to detected signals at the level of a few micro Jy at JVLA and GMRT frequencies. The details of our mm observations of the sGRB 140903A taken at 86.74 GHz are tabulated in Table 2. Spectroscopy of the afterglow was also performed using the 10.4 m GTC and the redshift value determined was ∼0.351 (Troja et al. 2016) consistent with that reported by Cucchiara et al. (2014). Using the measured redshift of this burst (Troja et al. 2016) and the γ-ray fluence by Palmer et al. (2014b), the isotropic-equivalent gamma-ray energy is $E_{\rm iso} \sim 0.04 \times 10^{51}$ erg (20–10^4 keV, rest-frame).

As a part of this work, *ISO*N-Kislovodsk SANTEL-400A optical telescope started observations ∼0.141d after the burst and did not see any afterglow down to a limiting magnitude of ∼18.6 mag (Pozanenko et al. 2014). To search further for the optical afterglow or for any possible 'kilonova' emission for this nearby sGRB, we observed the field of GRB 140903A with the 1.5 m AZT-22 telescope of Maidanak astronomical observatory on 2014 September 4, 6, 7, and 13, taking 12–15 images of 60 s exposure in the *R*-filter. All images were processed using NOAO's IRAF software package. The position of the optical source is in the wing of a bright star SDSS J155202.58 + 273611.7 (R = 12.9 mag). The limiting magnitude for every epoch far away from the bright star was obtained using nearby SDSS stars. To find a possible afterglow, we subtracted the combined image obtained on 2014 September 13 from that of 2014 September 4. At the position of the afterglow in the residual image, we do not find any source implying an equivalent upper limit variability of the source less than 0.5 mag (3σ) between the two epochs. This is in agreement with observations by Xu et al. (2014a) and confirms the absence of an afterglow signature 30 h after the burst trigger. Based on our present observations, we can also exclude the possibility of an underlying 'kilonova' brighter than $R \sim 22.0$ (3σ) at 10d associated with sGRB 140903A. The corresponding limiting value of the luminosity for the given redshift $L_R < 6.5 \times 10^{27}$ erg s^{-1} Hz^{-1} seems afterglow dominated and brighter by a factor of 6 than any GW170817 like associated 'kilonova' at similar epochs (Rossi et al. 2019).

A6 sGRB 140930B

Swift detected sGRB 140930B (trigger = 614094) on 2014 September 30 at 19:41:42 UT with a duration of T_{90} = 0.84 ± 0.12s (Baumgartner et al. 2014; De Pasquale et al. 2014b). The burst was also observed by *Konus* − *Wind* with the light curve having a complex multipulsed structure with a duration of ∼1.0s and the emission was seen up to ∼10 MeV (Golenetskii et al. 2014). The time-averaged spectrum of the burst (measured by *Konus* − *Wind* from T0 to T0 + 8.448s) had a best fit in the 20 keV − 15 MeV range by a power law with exponential cut-off model with $E_{\rm peak} = 1302^{+2009}_{-459}$ keV and total fluence of $8.1^{+5.1}_{-2.5} \times 10^{-6}$ erg cm^{-2} (Golenetskii et al. 2014). Since the redshift z of the sGRB 140930B is unknown, the trajectory of sGRB 140930B on the Amati diagram as a function of z (Fig. 9, see also Minaev et al. 2012) can be constructed using the fluence and $E_{\rm peak}(1+z)$ estimates. It follows from Fig. 9 that the trajectory does not cross the correlation region

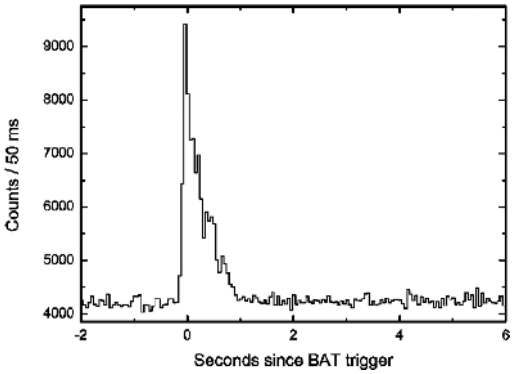

Figure A5. Light curve of sGRB 140930B obtained by SPI-ACS *INTEGRAL* in energy range 0.1–10 MeV with 50 ms time bins as a part of this study. On *x*-axis time since BAT trigger is shown, on *y*-axis counts per 50 ms are presented.

and lies above those drawn for lGRBs, which may suggest that sGRB 140930B belongs to the class of short bursts. The higher $E_{\rm peak}$ value confirms that the burst is spectrally hard. Overall a FRED light curve with three pulses after the main peak is visible in SPI-ACS *INTEGRAL* (Fig. A5). The SPI-ACS *INTEGRAL* off-set is 67 deg. There is no EE in either BAT (Baumgartner et al. 2014) or SPI-ACS *INTEGRAL* light curves. At a time scale of 50 s, the upper limit on EE activity in SPI-ACS for sGRB 140930B is ∼7300 counts; i.e. $S_{\rm EE} \sim (7.3 \times 10^{-7}$ erg cm$^{-2})$ at the 3σ significance level in the (75, 1000) keV range. *Fermi*-/GBM could not observe the burst as the satellite was passing in its South Atlantic Anomaly.

Early time optical observations using *Swift* UVOT (Breeveld & De Pasquale 2014), MASTER-II (Gorbovskoy et al. 2014), and 1.23m CAHA (Gorosabel, Hellmich & Mottola 2014) do not reveal any optical afterglow down to a limiting magnitude of $R \sim$21.1 mag. UAFO ORI-65 and *ISO*N-Kislovodsk SANTEL-400A telescopes started observations around 0.025 and 0.029d after the burst and did not see any afterglow down to a limiting magnitude of ∼16.1 and 20.4 mag, respectively (Polyakov et al. 2014). However, starting ∼3 h after the burst 4.2 m WHT found an optical source (Tanvir et al. 2014) that decayed in later images obtained by the 6.5m MMT (Fong et al. 2014b) and the 2.2m GROND (Graham et al. 2014) telescopes. The spectroscopic observations using Gemini-south were reported by Cenko et al. (2014) and the afterglow candidate was also observed in J and $K_{\rm s}$ bands using Keck-MOSFIRE (Perley & Jencson 2014).

We started to observe the field of GRB 140930B on 2014 October 3 at 22:58:33 UT, i.e. ∼3.1d after the trigger taking 13 frames with an exposure of 60 s in the r filter under mean FWHM of 0.8 arcsec using GTC 10.4 m. The refined position of the optical and infrared afterglow is strongly affected by a spike from nearby bright star S1 (J002523.61 + 241727.0, $r \sim$ 13.1 mag). All bright stars in the frames from GTC have six symmetrical spikes from a secondary mirror mount. We found the central position of the S1 star and then we rotated the combined image around this position 60 deg clockwise, to use a rotated image as a template for subtraction of the spike contaminating the position of the afterglow. In the resulting image we do not find any source at the position of the optical afterglow down to limiting magnitude of $r \sim$ 24.5 mag. The finding chart locating the XRT error circle is shown in Fig. A6 based on the late time data taken by the GTC 10.4 m. At the epoch of our GTC observations, limiting value of afterglow luminosity would be $L_r < 1.3 \times 10^{27}$ erg s^{-1} Hz^{-1} for an assumed redshift of

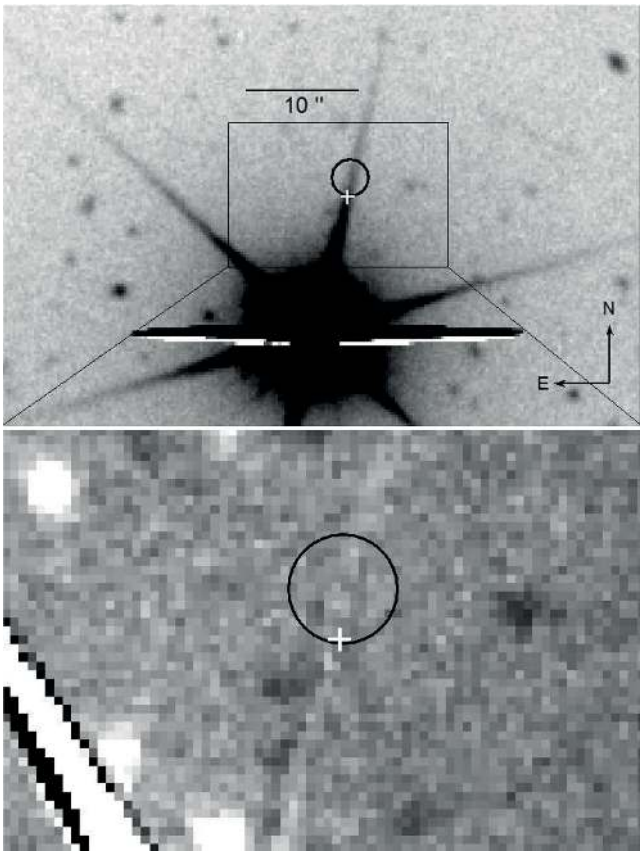

Figure A6. Finding chart of sGRB 140930B in the stacked frame of *r* band observed by GTC 10.4 m telescope. The XRT error box shown in the black circle is overlapped with one of the spikes of the nearby bright star. In the bottom panel, the zoomed portion (inset) is shown after applying image subtraction and the '+' sign marks the position of the afterglow reported by Tanvir, Levan & Fraser (2014).

$z \sim 0.5$. This value is nearly similar to the expected luminosity of GW170817 like 'kilonova' at similar epochs (Rossi et al. 2019).

Also, as a part of this study, the 4.2m WHT/ACAM and Gemini North/GMOS-N photometric data of the optical afterglow (Tanvir et al. 2014) were analysed. The results based on our multiband photometry using the 4.2 m WHT, the Gemini North, and GTC 10.4 m are reported in Table 5. The photometry was performed using NOAO's IRAF software package and calibrated using nearby SDSS stars. The *r*-band photometry from this study, along with those given in the GCN (Fong et al. 2014b; Graham et al. 2014), was used to produce the afterglow light as shown in Fig. A7. The temporal flux decay index using the *r*-band light curve was derived as $\alpha_o = 0.85 \pm 0.26$ during 0.13 to 1.65d after the burst. The contemporaneous *Swift* XRT light-curve decay index is $\alpha_X = 1.6 \pm 0.1$, where as X-ray spectral index $\beta_X = -0.71 \pm 0.15$. Assuming the cooling break frequency ν_c lying between the two observed bands, the closure relations in case of the *ISM* afterglow model (Sari et al. 1998) are broadly consistent with the observed values of temporal decay at optical bands whereas the temporal decay index at X-rays are steeper than the expected model predictions. GTC 10.4 m was further triggered to search for any possible host galaxy on 2018 December 10 and a total of 30 images of 120s each were acquired (see Table 5) in the *r* band. In the stacked image, we do not see any object down to a limiting magnitude of ∼24.8 mag at the location of the afterglow after accounting for the possible effects of the nearby bright star. So, it is concluded that the host galaxy of the sGRB 140930B would be fainter than $r \sim 24.8$ mag.

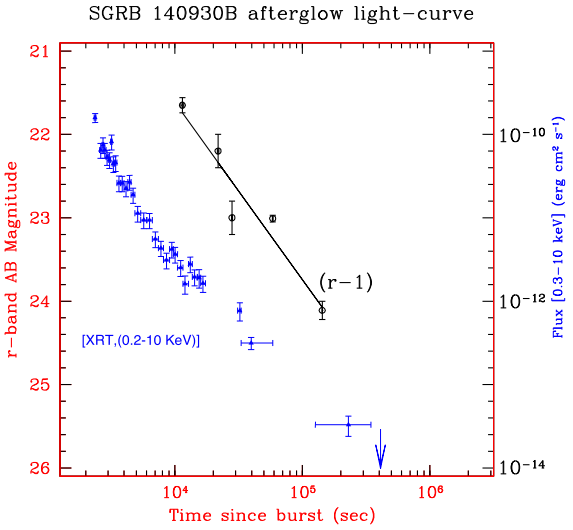

Figure A7. sGRB 140930B afterglow optical *r* band afterglow light curve. The solid black curve is the best-fitting power-law model to the *r*-band light curve. The two *r*-band data points around 2×10^4 s (Fong et al. 2014b) and 3×10^4 s (Graham et al. 2014) post-burst are from GCN circular archive, considered while fitting the power law to derive the temporal decay index. For comparison, *Swift* XRT light curves are also plotted in blue colour.

A7 sGRB 141212A

sGRB 141212A was discovered on 2014 December 12 at 12:14:01 UT by the *Swift*-BAT (Ukwatta, Barthelmy & Beardmore 2014). The BAT light curve shows a single spike with a duration of about 0.1 s in the energy range (25–350) keV. In the soft energy channel 15–25 keV a second pulse is clearly visible with a duration of 0.1s at 0.3s after the trigger. The duration parameter T_{90} in the 15–350 keV energy range is 0.30 ± 0.08s (Palmer et al. 2014a). The time-averaged spectrum from T+0.00 to T + 0.34s is best fit by a simple power-law model with power-law index of 1.61 ± 0.23. The fluence in the 15–150 keV band is $7.2 \pm 1.2 \times 10^{-08}$ erg cm^{-2} (Palmer et al. 2014a). GRB 141212A was also found in *INTEGRAL* SPI-ACS data (there was no IBAS trigger) as a single pulse with duration of 0.15 s and statistical significance of 7.3σ (Fig. A8). The second soft pulse is not visible in SPI-ACS, which is sensitive above ∼80 keV. At a time-scale of 50s, the upper limit on EE activity in SPI-ACS for sGRB 141212A is ∼7300 counts i.e. $S_{EE} \sim (7.3 \times 10^{-7}$ erg cm$^{-2})$ at the 3σ significance level in the (75, 1000) keV range. Ground-based MITSuME (Fujiwara et al. 2014), MASTER network of telescopes (Gres et al. 2014), and UVOT onboard *Swift* did not find any new optical source within the XRT error-box in the images taken around 31s, 46s, and 72s after the BAT trigger, respectively, down to a limiting magnitude of $V \sim 19$ mag.

We started observation of the sGRB 141212A with the 1.5 m AZT-33-IK telescope at Mondy observatory on 2014 December 12 at 12:36:10.7650 UT, i.e. 22 min after the trigger. We also observed it later with the same telescope on December 14 and December 18. We also observed the field with the 0.4m telescope at Khureltogot observatory and 1.0m telescope at Tien Shan observatory (see Table 5 for the complete log of observations). The host galaxy suggested by Malesani et al. (2014) was also detected from our observations using 1.0–1.5 m telescopes. We did not find any evidence for the optical

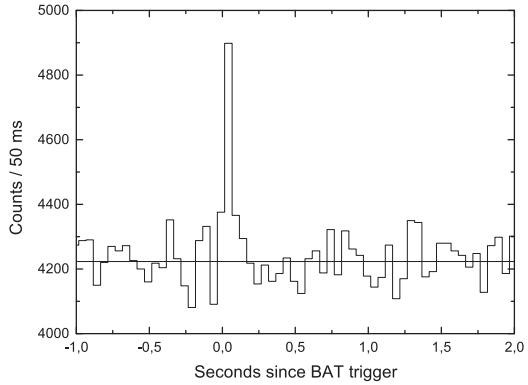

Figure A8. Light curve of sGRB 141212A from *INTEGRAL* SPI-ACS data in the energy range 0.1–10 MeV with 50 ms time resolution. The *x*-axis is time since BAT trigger, and the *y*-axis is counts in 50 ms time bins. The thin horizontal line represents the background level.

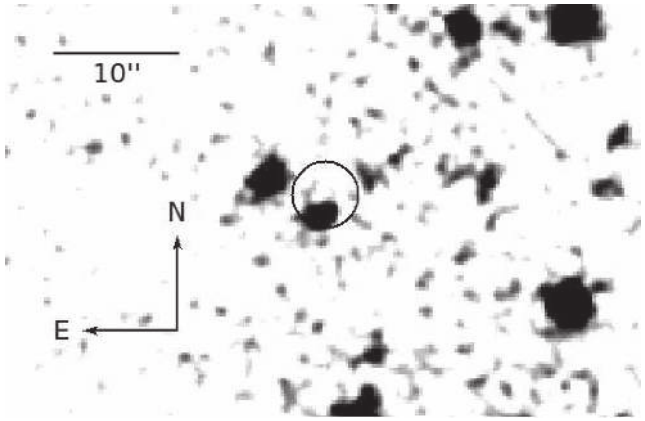

Figure A9. Finding chart of sGRB 141212A in the stacked frame of *r*-band data obtained with the GTC 10.4 m telescope. The XRT error box is shown as a black circle. The bright host galaxy is also visible within the XRT error circle.

afterglow signature in our observations taken in *R* filter. As a part of the present analysis, a deeper photometric data using Gemini-N/GMOS-N 8.0 m (Gemini program ID = GN-2014B-Q-10) data in the *i* band was analyzed and the bright host galaxy candidate was clearly detected in the data taken at the two epochs as listed in Table 5. Using the Gemini-N/GMOS-N *i* band data, the possibility of any point source in the vicinity of the host galaxy candidate (Malesani et al. 2014) is ruled out up to a limiting magnitude of $i \sim 26$ mag (3σ) at 0.68d post-burst. This deep limiting value translates to a luminosity of $L_i < 5 \times 10^{26}$ erg s^{-1} Hz^{-1} (a factor of 3 deeper than rest-frame luminosity of GW170817 like 'kilonova' at contemporaneous epochs), further implies that at the epoch of our observations in the *i* band, any associated GW170817 like 'kilonova' with the burst would have been detected as seen in a few cases of sGRBs in Rossi et al. (2019).

As a part of this study, multiband photometry with the 10.4 m GTC in *gri*-filters was performed at late epochs i.e. around 427.3d post-burst to investigate properties of the host galaxy (see Table 5). The finding chart with the XRT error circle superimposed on the data taken by the GTC 10.4 m is shown in Fig. A9. The observed flux of the host galaxy of sGRB 141212A obtained by 10.4 m GTC in different filters (see Table 5) and the suggested redshift of the burst $z = 0.596$ (Chornock et al. 2014) allowed us to model the SED of the host galaxy. We also added upper limits in filters *u* and *b* from *Swift*-UVOT data (Oates & Ukwatta 2014). To build the SED of the host galaxy of sGRB 141212A and to estimate parameters, we used the LEPHARE software package (Arnouts et al. 1999; Ilbert et al. 2006) with fixed redshift. We used the PEGASE2 population synthesis models library to obtain the best-fitting SED, the mass and the age of the galaxy, and star formation rate. We tested four different reddening laws: the MW extinction law by Seaton (1979), LMC (Fitzpatrick 1986), SMC (Prévot et al. 1984), and the reddening law for starburst galaxies (Calzetti et al. 2000; Massarotti et al. 2001). The reduced χ^2, galaxy morphological type, bulk extinction, absolute rest-frame *B* magnitude, age, mass, star formation rate, and specific star formation rate (SSFR) per unit galaxy stellar mass are listed in Table A1 for all four tested extinction laws. Fig. A10 represents the best model corresponding to the MW extinction law.

The best fit shows that the host is a galaxy of elliptic type with $M_B = -19.9$ mag and a moderate linear size along the major axis about 13 kpc. The major axis is oriented 45 deg North-West. Age of the host galaxy is ∼2 Gyr, and the average internal extinction in the galaxy is rather high, $E(B-V) = 0.50$ mag. The host galaxy has a mass of $\sim 9 \times 10^9$ M$_\odot$, and a high star formation rate of SFR ∼50 M$_\odot$/yr. All obtained parameters are in a good agreement with previous studies by Chrimes et al. (2018) except for SFR, which is two orders higher in our results.

A8 sGRB 151228A

sGRB 151228A (trigger = 668543) was discovered by *Swift* on 2015 December 28 at 03:05:12 UT with a duration of $T_{90} = 0.27 \pm 0.01$s (Barthelmy et al. 2015; Ukwatta, Barthelmy & Cummings 2015). The burst was also detected by *Fermi*-GBM (Bissaldi, Zhang & Veres 2015), but there was no *Swift*-XRT localization (Page 2015) due to an observing constraint. The burst was also detected by *INTEGRAL* SPI-ACS and triggered its IBAS system. The SPI-ACS light curve of sGRB 151228A is presented in Fig. A11 (top panel) and shows two overlapping pulses with a total duration of about ∼0.3 s. At a time-scale of 50s, the upper limit on EE activity in SPI-ACS for sGRB 151228A is ∼7700 counts i.e. $S_{EE} \sim (7.7 \times 10^{-7}$ erg cm$^{-2})$ at the 3σ significance level in the (75, 1000) keV range. As a part of the present analysis, *Fermi*-GBM data were fitted for the time-averaged spectrum of the NaI n4 data and it was found that cutoff-PL model as the best fit. The low-energy photon index $= 0.72 \pm 0.84$ and $E_{peak} = 261.18^{+164.94}_{-58.28}$ keV, much lower than reported in Bissaldi et al. (2015). The corresponding GBM flux is $(1.4^{+1.39}_{-0.61}) \times 10^{-6}$ erg cm^{-2} s^{-1} in 1–10^4 keV. The light curve of *Fermi*-GBM also has two overlapping pulses with a total duration of about ∼0.4 s. The spectral fitting plot with cutoff-PL model is shown in Fig. A11 (bottom panel).[4] As estimated in case of sGRB 140930B, we constructed the trajectory for sGRB 151228A on the Amati diagram (see Fig. 9), because the redshift *z* for sGRB 151228A was unknown. The trajectory lies above the main correlation at any *z*, which may suggest that sGRB 151228A belongs to the class of the short bursts. Since the burst does not fall into the $E_{peak}(1+z)/E_{iso}$ correlation region at any *z*, the redshift and E_{iso} of this burst cannot be estimated.

Early optical searches within the BAT error circle do not find any new optical source down to a limiting magnitude of ∼17 mag using the 0.60m T60 telescope (TUBITAK National Observatory,

[4]https: //fermi.gsfc.nasa.gov/ssc/data/analysis/rmfit/

Table A1. sGRB 141212A host galaxy properties derived from the SED fitting.

Fitted parameters	Starburst model	MW model	LMC model	SMC model
χ^2/DOF	2.8/3	2.7/3	2.8/3	5.9/3
Type	E	E	E	S0
$E(B-V)$, mag	0.50	0.50	0.50	0.00
M_B, mag	−19.9	−19.9	−19.9	−19.7
Age, Gyr	$2.65^{+2.50}_{-0.11}$	$2.23^{+1.70}_{-0.09}$	$2.05^{+3.44}_{-0.13}$	$3.10^{+0.09}_{-0.25}$
Mass, $(\times 10^{10})\,M_\odot$	$1.0^{+5.4}_{-0.7}$	$0.9^{+3.7}_{-0.6}$	$0.9^{+8.5}_{-0.7}$	$1.4^{+12.6}_{-0.8}$
SFR, $M_\odot$/yr	87^{+343}_{-70}	48^{+147}_{-41}	49^{+155}_{-36}	$4.2^{+85.5}_{-1.5}$
SSFR, $(\times 10^{-10})$yr^{-1}	88^{+270}_{-65}	55^{+173}_{-46}	56^{+215}_{-49}	$2.9^{+73.6}_{-0.4}$

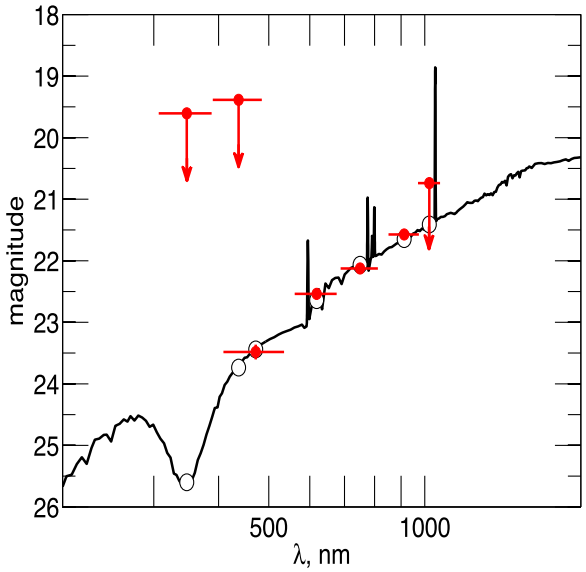

Figure A10. The SED (line) of the host galaxy of sGRB 141212A fitted by the LEPHARE with fixed redshift $z = 0.596$. Filled red circles depict, respectively, the data points in the *Swift*/UVOT filters u, b, taken from Oates & Ukwatta (2014), g, r, i from original observations (see Table 5), and z, y from Chrimes et al. (2018, Table A1). Open circles represent model magnitudes for each filter. All magnitudes are in AB system.

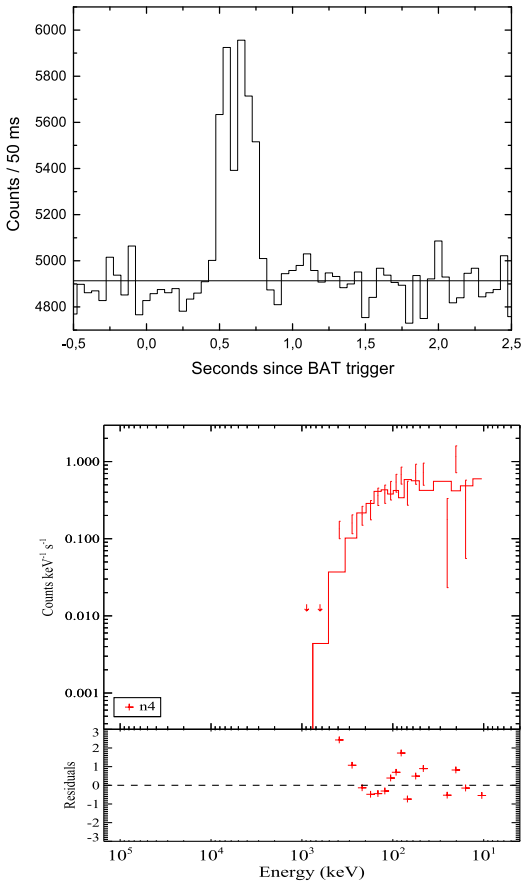

Figure A11. Light curve of sGRB 151228A from *INTEGRAL* SPI-ACS in the energy range 0.1–10 MeV with 50 ms time resolution. The x-axis is time since BAT trigger, and the y-axis is counts in 50 ms time bins (top panel). The thin horizontal line represents the background level. The best-fitting model of the prompt emission spectra of the *Fermi*-GBM (bottom panel) data of sGRB 151228A in counts.

Antalya, Turkey) starting 90 s after the burst (Sonbas et al. 2015). The GTC 10.4 m was triggered around ∼1.143d after the burst and covered the full error box in i filter with a total exposure time of 5 × 60 s. The GTC observations cover the full BAT error circle, except for a gap between chips of a CCD camera (the gap covers ∼7.4 per cent of the total error box). The BAT error-circle was again observed by the GTC 10.4m in i filter around 69d after the burst with a total exposure of 7 × 75 s. Due to different limiting magnitude, FWHM, and inadequate flat-fielding for the whole FOV of the CCD camera, we could not use image subtraction method to search for the source at the first epoch. Instead, we performed a catalogue extraction at S/N = 3 for each epoch. We did not find any new object at the first epoch down to a limiting magnitude of >23.7 mag comparing with the second epoch (limiting magnitude for the second epoch was 24.8 mag). The results of our photometry and values of the limiting magnitude for sGRB 151228A are reported in Table 5.

[1]*Aryabhatta Research Institute of Observational Sciences, Manora Peak, Nainital 263 002, India*
[2]*Instituto de Astrofisica de Andalucia (IAA-CSIC), Glorieta de la Astronomia s/n, E-18008, Granada, Spain*
[3]*Unidad Asociada Departamento de Ingeniería de Sistemas y Automática, E.T.S. de Ingenieros Industriales, Universidad de Málaga, E-29071, Spain*

[4]*Unidad Asociada Grupo Ciencias Planetarias UPV/EHU-IAA/CSIC, Departamento de Fisica Aplicada I, E.T.S., Universidad del Pais Vasco UPV/EHU, Bilbao, E-48071, Spain*
[5]*Ikerbasque, Basque Foundation for Science, Bilbao, E-48013, Spain*
[6]*Nikolaev National University, Nikolska 24, Nikolaev 54030, Ukraine*
[7]*Nikolaev Astronomical Observatory, Nikolaev, Ukraine*
[8]*Institute for Science and Technology in Space, SungKyunKwan University, Suwon 16419, Korea*
[9]*Astronomical Institute of the Academy of Sciences, Boční II 1401, CZ-14100 Praha 4, Czech Republic*
[10]*Universidad de Jaén, Campus Las Lagunillas, s/n, Jaén, E-23071, Spain*
[11]*Institute de Radioastronomie Millimétrique (IRAM), 300 rue de la Piscine, F-38406 Saint Martin d'Hères, France*
[12]*Space Research institute, Moscow, Russia*
[13]*National Research Nuclear University MEPhI (Moscow Engineering Physics Institute), Moscow, Russia*
[14]*Thuringer Landessternwarte, Tautenburg, Germany*
[15]*Special Astrophysical Observatory, Nizhniy Arkhyz, Zelenchukskiy region, Karachai-Cherkessian Respublic, 369167, Russia*
[16]*Department of Physics, University of Adiyaman, 02040 Adiyaman, Turkey*
[17]*Instituto de Astrofśica de Canarias (IAC), Vía L'actea s/n, 38205 Santa Cruz de La Laguna, Tenerife, Spain*
[18]*School of Earth and Space Exploration, Arizona State University, Tempe, AZ 85287, USA*
[19]*NASA, Goddard Space Flight Center, Greenbelt, MD 20771, USA*
[20]*Radio Astronomy Laboratory of the Crimean Astrophysical Observatory, Katsiveli, Crimea*
[21]*Kharadze Abastumani Astrophysical Observatory of Ilya State University, K. Cholokashvili Ave. 3/5, Tbilisi 0162, Georgia*
[22]*Ulugh Beg Astronomical Institute of the Uzbek Academy of Sciences, Tashkent, Usbekistan*
[23]*Fesenkov Astrophysical Institute, Almaty, Kazakhstan*
[24]*Astronomical Scientific Center, Moscow, Russia*
[25]*Ussuriysk Astrophysical observatory of Far-East Department of Russian Academy of Sciences, Ussuriysk, Russia*
[26]*Kuban State University, Krasnodar, Russia*
[27]*Istanbul University Science Faculty, Department of Astronomy and Space Sciences, 34119, University-Istanbul, Turkey*
[28]*Instituto de Astronomia, UNAM, Unidad Academica en Ensenada. Ensenada 22860 Mexico*
[29]*University of Leicester, Department of Physics & Astronomy and Leicester Institute of Space & Earth Observation, University Road, Leicester LE1 7RH, UK*
[30]*Astronomy Department, University of California, Berkeley, CA 94720-7450, USA*
[31]*Department of Astronomy and Astrophysics, University of California, 1156 High Street, Santa Cruz, CA 95064, USA*
[32]*Institute of Solar-Terrestrial Physics, Irkutsk, Russia*
[33]*Yunnan National Astronomical Observatory, Chinese Academy of Sciences, Phoenix Hill, 650011 Kunming, Yunnan, China*
[34]*Beijing National Astronomical Observatory, Chinese Academy of Sciences, 20A Datun Road, Chaoyang District, Beijing 100012, China*
[35]*Center of Astronomy and Geophysics Mongolian Academy of Sciences, Ulaanbaatar, Mongolia*
[36]*National Research University Higher School of Economics, Moscow 101000, Russia*
[37]*Keldysh Institute of Applied Mathematics, Moscow, Russia*
[38]*INAF - Istituto di Astrofisica e Planetologia Spaziali, Via Fosso del Cavaliere 100, 00133 Roma, Italy*
[39] *Key Laboratory of Modern Astronomy and Astrophysics, Nanjing University, Ministry of Education, Nanjing, 210093, China*
[40]*School of Astronomy and Space Science, Nanjing University, 210093, Nanjing, China*
[41]*Department of Physics, University of Warwick, Coventry CV4 7AL, UK*
[42]*Department of Physics, University of Bath, Claverton Down, Bath BA2 7AY, UK*
[43]*Samtskhe Javakheti State university, Rustaveli st.113, Akhaltsikhe, 0080, Georgia*
[44]*Instituto de Astronomía, Universidad Nacional Autónoma de Mèxico, Apartado Postal 70-264, 04510 México, CDMX, Mexico*

This paper has been typeset from a TEX/LATEX file prepared by the author.